AGU PUBLICATIONS

JGR

Journal of Geophysical Research: Atmospheres

RESEARCH ARTICLE
10.1002/2016JD025455

Key Points:
- O_3 photochemistry and temperature control clumped isotopes in atmospheric O_2
- Stratospheric and tropospheric Δ_{36} signatures are distinct
- Circulation-sensitive distribution of tropospheric O_3 controls tropospheric Δ_{36}

Supporting Information:
- Supporting Information S1

Correspondence to:
L. Y. Yeung,
lyeung@rice.edu

Citation:
Yeung, L. Y., et al. (2016), Isotopic ordering in atmospheric O_2 as a tracer of ozone photochemistry and the tropical atmosphere, *J. Geophys. Res. Atmos.*, *121*, 12,541–12,559, doi:10.1002/2016JD025455.

Received 1 JUN 2016
Accepted 3 OCT 2016
Accepted article online 5 OCT 2016
Published online 26 OCT 2016

Isotopic ordering in atmospheric O_2 as a tracer of ozone photochemistry and the tropical atmosphere

Laurence Y. Yeung[1], Lee T. Murray[2,3,4], Jeanine L. Ash[5], Edward D. Young[5], Kristie A. Boering[6], Elliot L. Atlas[7], Sue M. Schauffler[8], Richard A. Lueb[8], Ray L. Langenfelds[9], Paul. B. Krummel[9], L. Paul Steele[9], and Sebastian D. Eastham[10]

[1]Department of Earth Science, William Marsh Rice University, Houston, Texas, USA, [2]NASA Goddard Institute for Space Studies, New York, New York, USA, [3]Lamont-Doherty Earth Observatory, Columbia University, Palisades, New York, USA, [4]Now at Department of Earth and Environmental Sciences, University of Rochester, Rochester, New York, USA, [5]Department of Earth, Planetary, and Space Sciences, University of California, Los Angeles, California, USA, [6]Departments of Chemistry and Earth and Planetary Science, University of California, Berkeley, California, USA, [7]Division of Marine and Atmospheric Chemistry, University of Miami, Miami, Florida, USA, [8]National Center for Atmospheric Research, Boulder, Colorado, USA, [9]CSIRO Oceans and Atmosphere, Aspendale, Victoria, Australia, [10]Laboratory of Aviation and the Environment, Department of Aeronautics and Astronautics, Massachusetts Institute of Technology, Cambridge, Massachusetts, USA

Abstract The distribution of isotopes within O_2 molecules can be rapidly altered when they react with atomic oxygen. This mechanism is globally important: while other contributions to the global budget of O_2 impart isotopic signatures, the $O(^3P) + O_2$ reaction resets all such signatures in the atmosphere on subdecadal timescales. Consequently, the isotopic distribution within O_2 is determined by O_3 photochemistry and the circulation patterns that control where that photochemistry occurs. The variability of isotopic ordering in O_2 has not been established, however. We present new measurements of $^{18}O^{18}O$ in air (reported as Δ_{36} values) from the surface to 33 km altitude. They confirm the basic features of the clumped-isotope budget of O_2: Stratospheric air has higher Δ_{36} values than tropospheric air (i.e., more $^{18}O^{18}O$), reflecting colder temperatures and fast photochemical cycling of O_3. Lower Δ_{36} values in the troposphere arise from photochemistry at warmer temperatures balanced by the influx of high-Δ_{36} air from the stratosphere. These observations agree with predictions derived from the GEOS-Chem chemical transport model, which provides additional insight. We find a link between tropical circulation patterns and regions where Δ_{36} values are reset in the troposphere. The dynamics of these regions influences lapse rates, vertical and horizontal patterns of O_2 reordering, and thus the isotopic distribution toward which O_2 is driven in the troposphere. Temporal variations in Δ_{36} values at the surface should therefore reflect changes in tropospheric temperatures, photochemistry, and circulation. Our results suggest that the tropospheric O_3 burden has remained within a ±10% range since 1978.

1. Introduction

Global patterns of atmospheric circulation have changed dramatically with climate in the past [*Mayewski et al.*, 1997; *Vecchi et al.*, 2006; *Eagle et al.*, 2013; *Oster et al.*, 2015]. They are expected to change in the future, but accurately predicting the changes in heat and moisture transport, trace gases, and climate sensitivity remains a challenge [*Schneider et al.*, 2010; *Shepherd*, 2014; *Sherwood et al.*, 2014; *Bony et al.*, 2015]. The paleoclimate record of circulation could be a guide; it is typically inferred from the analysis of hydroclimate [*Wang et al.*, 2008; *Yoshimura et al.*, 2008; *Risi et al.*, 2010] and mineral dust records [*Mayewski et al.*, 1997]. However, these records tend only to represent patterns of variability at the surface. The record of dynamic "vertical" properties of the atmosphere such as the strength of tropical upwelling must be inferred from these horizontal patterns using general circulation models [*Haigh*, 1996; *Shindell et al.*, 2001; *Partin et al.*, 2007; *Schneider et al.*, 2010; *Tripati et al.*, 2014]. These inferences are difficult to test given the paucity of geological records for these processes, so their behavior on climatically relevant timescales is not well known. In this manuscript, we explore the viability of clumped isotopes in O_2 as a tracer of atmospheric chemistry and physics on decadal and longer timescales.

The tracer—the proportional abundance of $^{18}O^{18}O$ in O_2, quantified as the Δ_{36} value—is sensitive to thermal and photochemical properties of the atmosphere (Figure 1). Ozone photochemistry (or, more precisely, the $O(^3P) + O_2$ isotope exchange reaction) drives the proportions of $^{18}O^{18}O$ and $^{17}O^{18}O$ toward isotopic

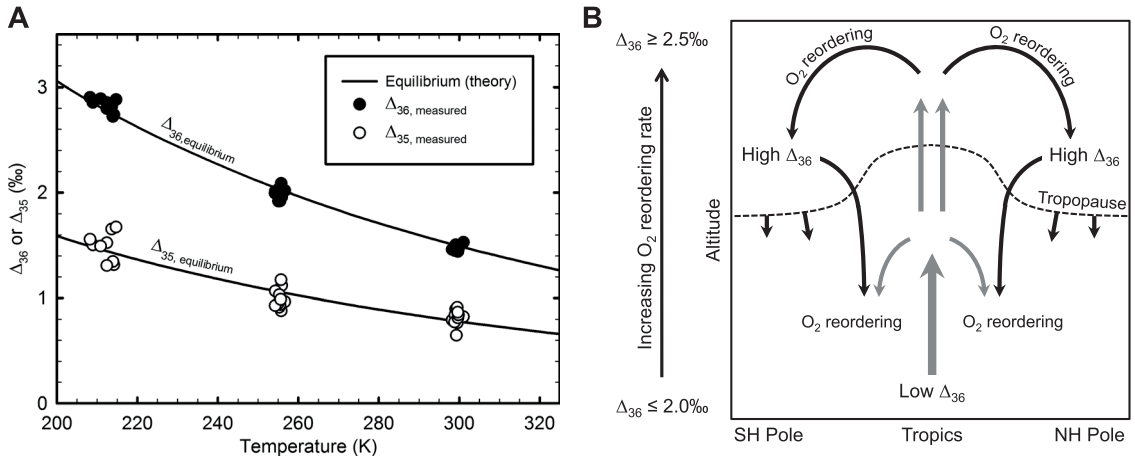

Figure 1. Factors controlling isotopic ordering in O_2 on decadal timescales. (a) Photochemically catalyzed $O(^3P) + O_2$ isotope exchange equilibrium yields nonstochastic enrichments in $^{18}O^{18}O$ and $^{17}O^{18}O$ (shown as Δ_{36} and Δ_{35} values). Data points from the instrument at Rice University are compared with theoretical predictions for the equilibrium temperature dependence. (b) Schematic of the atmospheric Δ_{36} budget. Oxygen isotope exchange reactions occur throughout the atmosphere, but the rates of reaction generally increase with altitude. Also, temperature decreases with altitude and transport mixes air from different altitudes. Therefore, the Δ_{36} budget is characterized by O_2 isotope exchange reactions occurring at different temperatures, modulated by air mass mixing. The troposphere has Δ_{36} values that reflect the balance of photochemical isotope exchange kinetics (i.e., locally incomplete isotopic equilibration), tropospheric circulation, and STT. Biological cycling of O_2 has negligible effects on the global Δ_{36} budget on decadal timescales.

equilibrium. Subtle differences in vibrational energies of the O_2 isotopologues favors $^{18}O^{18}O$ and $^{17}O^{18}O$ formation moreso than chance alone would dictate. As temperatures decrease, the preference for $^{18}O^{18}O$ formation increases by 0.010‰/K to 0.024‰/K at Earth surface temperatures, resulting in equilibrium Δ_{36} values that range from 1.49‰ to 3.06‰ between 300 K and 200 K, respectively (see Figure 1a; excesses in $^{17}O^{18}O$—i.e., Δ_{35} values—are about half those for $^{18}O^{18}O$ at equilibrium) [*Wang et al*., 2004]. Ozone photochemistry in cold regions of the atmosphere tends to increase Δ_{36} values, while O_3 photochemistry in warmer regions tends to decrease Δ_{36} values, within these limits. The approach to local isotopic equilibrium in the atmosphere is kinetically limited by $O(^3P)$ concentrations, which can vary by many orders magnitude depending on altitude [*Yeung et al*., 2014].

In the stratosphere, O_3 photochemistry rearranges the isotopes in O_2 on timescales of months or less toward $\Delta_{36} \geq 2.3$‰, corresponding to stratospheric temperatures below ~240 K [*Yeung et al*., 2012, 2014]. In the troposphere, O_3 photochemistry rearranges isotopes in O_2 as well, but orders of magnitude more slowly and at warmer temperatures (Figure 1b). This contrast has two consequences. First, Δ_{36} values are lower in the troposphere because isotope reordering generally occurs at warmer temperatures. Second, tropospheric Δ_{36} values reflect the balance of tropospheric and stratospheric processes—both photochemical and dynamical—that can vary on a range of timescales.

The spatial patterns of O_3 photochemistry determine tropospheric and stratospheric contributions to the atmospheric Δ_{36} budget. They are driven by precursor emissions as well as mass transport. Regions of deep convection in the midlatitudes, for example, are associated with mass exchange between the surface and the lowermost stratosphere that has global consequences for the budget of O_3 [*Stohl et al*., 2003; *Wu et al*., 2007; *Škerlak et al*., 2014; *Barth et al*., 2015]. The distribution of these features, as well as others that transport O_3 and its precursors, affect atmospheric Δ_{36} values by determining the rates and temperatures at which Δ_{36} values are reset.

Evidence for the importance of the O_3 distribution in the troposphere can be found in the measured Δ_{36} values at the surface. Air in Los Angeles had a Δ_{36} value of 1.97 ± 0.07‰ in 2012–2014 (2 SE, $n = 23$), corresponding to an effective temperature of 260 ± 5 K [*Yeung et al*., 2014]. This temperature is significantly colder than local mean-annual temperatures (290 K), yet warmer than typical stratospheric temperatures. While stratosphere-troposphere exchange (STE) and mixing is undoubtedly important, patterns of O_3 photochemistry in the free troposphere, which are governed by surface emissions and atmospheric circulation, may play a primary role in determining tropospheric Δ_{36} values. Increasing rates of O_3 photochemistry

near the surface, for example, would tend to drive tropospheric Δ_{36} values lower toward warmer effective temperatures, all else being equal.

Here we test the link between circulation, O_3, and Δ_{36} values in a combined observational and modeling study. We obtain empirical constraints on the global budget of clumped isotopes in O_2 using a new set of atmospheric Δ_{36} measurements, which we interpret with the aid of the GEOS-Chem global 3-D chemical transport model. We confirm that the primary control on Δ_{36} values in both the stratosphere and troposphere is the spatial pattern of O_3 photochemistry. In the stratosphere, Δ_{36} values resembling local equilibrium are associated with rapid isotope reordering and high concentrations of O_3. In the troposphere, patterns of O_2 isotope reordering rates are closely associated with features of the tropical overturning circulation. When integrated globally, these patterns explain the observed surface Δ_{36} values after including the effects of STE. Our modeling results indicate that anthropogenic effects on tropospheric O_3 concentrations over the past century may be detectable in the ice-core record of Δ_{36}. Furthermore, changes in free-troposphere temperatures may be detectable on longer timescales.

2. Methods

2.1. Clumped-Isotope Measurements

Isotopic ordering in O_2 is quantified in reference to the stochastic (random) distribution of isotopes according to the definition $\Delta_{36} = ({}^{36}R_{\mathrm{sample}}/{}^{36}R_{\mathrm{stochastic}} - 1)$, where ${}^{36}R_{\mathrm{sample}} = {}^{36}O_2/{}^{32}O_2$ and ${}^{36}R_{\mathrm{stochastic}} = ({}^{18}O/{}^{16}O)^2$. Similarly, $\Delta_{35} = ({}^{35}R_{\mathrm{sample}}/{}^{35}R_{\mathrm{stochastic}} - 1)$, where ${}^{35}R_{\mathrm{sample}} = {}^{35}O_2/{}^{32}O_2$ and ${}^{35}R_{\mathrm{stochastic}} = 2 \times ({}^{18}O/{}^{16}O) \times ({}^{17}O/{}^{16}O)$. Isotopologue measurements were performed at UCLA and Rice University after gas chromatographic separation of O_2 from other components of air according to established techniques [*Yeung et al*., 2012]. They were calibrated using photochemically and thermally catalyzed equilibrations of standard gases at known temperatures performed during the same analytical sessions [*Yeung et al*., 2014]. The theoretical equilibrium temperature dependence of Δ_{36} and Δ_{35} values are calculated from partition function ratios and harmonic vibrational frequencies for the O_2 isotopologues; they are likely accurate within 0.01‰ [*Wang et al*., 2004].

Measurements performed at UCLA have an external reproducibility of ±0.17‰ in Δ_{36} (1σ, on a ThermoScientific *MAT 253*) based on replicate analyses of air [*Yeung et al*., 2014], whereas measurements performed at Rice University on a high-resolution isotope ratio mass spectrometer (a modified Nu Instruments *Perspective IS*) had significantly better external reproducibility of ±0.038‰ in Δ_{36} (1σ). The latter reproducibility corresponds to the pooled standard deviation of 11 samples in this study that were analyzed in duplicate or triplicate at Rice (see Table S1 in the supporting information), which is similar to the instrumental uncertainty (1 SE for 2000s integration time using ion currents of 40 nA and 0.2 pA for ${}^{16}O{}^{16}O^+$ and ${}^{18}O{}^{18}O^+$, respectively).

We analyzed whole-air samples from the stratosphere and troposphere collected during three Northern Hemisphere field campaigns between 2000 and 2012: The SOLVE campaign in the boreal winter of 1999/2000 [*Newman et al*., 2002], a scientific balloon flight from Fort Sumner, NM (USA) in September 2004 [*Froidevaux et al*., 2006; *Wiegel et al*., 2013], and the DC3 campaign in the Southeastern USA in May/June 2012 [*Barth et al*., 2015]. Atmospheric samples were obtained as whole-air samples using the methods described in earlier publications [*Lueb et al*., 1975]. In addition, we measured subsamples of archived air from Cape Grim, Australia in the Southern Hemisphere between 1978 and 2013 [*Langenfelds et al*., 1996].

2.2. Two-Box Modeling of Atmospheric Δ_{36} Values

We employed the two-box model of the stratosphere and troposphere described in *Yeung et al*. [2012] to obtain insights into the budget of clumped isotopes in atmospheric O_2. Briefly, the tropospheric ${}^{18}O{}^{18}O$ budget can be represented by the following mass balance equation at steady state:

$$F_{\mathrm{ST}}\chi_{\mathrm{S}}^{36} - F_{\mathrm{TS}}\chi_{\mathrm{T}}^{36} + F_{\mathrm{P}}\chi_{\mathrm{P}}^{36} - F_{\mathrm{R}}\chi_{\mathrm{T}}^{36}\alpha_{36,\mathrm{R}} - E_{\mathrm{trop}}\left(\chi_{\mathrm{T}}^{36} - \chi_{\mathrm{Tequil}}^{36}\right) = 0 \quad (1)$$

with similar equations for the other O_2 isotopologues. The first and second terms represent isotopic fluxes due to STE, with F_{ST} and F_{TS} being the stratosphere-to-troposphere and troposphere-to-stratosphere fluxes of O_2, respectively. We used annual net mass fluxes of 4.6×10^{18} mol O_2 yr^{-1} obtained by applying the method of *Appenzeller et al*. [1996] on monthly mean air mass data. They are similar to literature estimates [*Schoeberl*, 2004] and allow our atmospheric simulations to be evaluated using their own transport schemes.

Biological cycling is expressed in the third and fourth terms, with F_P and F_R being the O_2 fluxes due to photosynthesis and respiration, respectively (3.43×10^{16} mol O_2 yr^{-1} [*Blunier et al*., 2012]). The fifth term represents the tropospheric equilibration flux of O_2, with E_{trop} being the tropospheric isotope exchange rate. The mole fractions χ represent end-member isotopologue abundances of mixing end-members (subscripts *S* and *T* for stratosphere and troposphere) and process signatures (subscripts *P* and T_{equil} for photosynthesis and tropospheric isotope equilibration). The α_R value is the isotopic fractionation factor for respiration. Generally, biological cycling terms are small because while biological cycling alters the isotopic composition in O_2 on centennial to millennial timescales [*Bender et al*., 1994; *Severinghaus et al*., 2009], the whole-troposphere O_2 reordering timescale is subdecadal [*Yeung et al*., 2012].

Assuming tropospheric O_2 is well mixed on annual timescales, equation (1) can be approximated by

$$F_{ST}\Delta_{36,strat} - F_{TS}\Delta_{36,trop} - E_{trop}\left(\Delta_{36,trop} - \Delta_{36,Tequil}\right) \approx 0 \quad (2)$$

in which $\Delta_{36,strat}$ is the end-member composition of stratospheric O_2 entering the troposphere, $\Delta_{36,trop}$ is the mean Δ_{36} value of tropospheric O_2, and $\Delta_{36,Tequil}$ is the whole-troposphere equilibration end-member (see section 2.3). The use of Δ_{36} values rather than mole fractions in equation (2) is reasonably accurate because isotope exchange reactions do not detectably alter the bulk isotopic composition of O_2; Δ_{36} values therefore vary linearly upon mixing. The approximate equation above illustrates the balance of stratospheric and tropospheric processes governing the Δ_{36} budget on annual timescales: Mass transport (first two terms) is balanced by tropospheric isotope reordering (third term). Biological cycling decreases the steady state $\Delta_{36,trop}$ value by ~0.01‰ [*Yeung et al*., 2015] and varies minimally on these timescales [*Severinghaus et al*., 2009].

2.3. Chemical Transport Modeling Using GEOS-Chem

GEOS-Chem (version 10-01d; http://www.geos-chem.org) is a global three-dimensional chemical transport model of atmospheric photochemistry and aerosols driven by assimilated meteorology from the NASA Global Modeling and Assimilation Office. Here we used both the Modern-Era Retrospective Analysis for Research and Applications (MERRA) [*Rienecker et al*., 2011] and the Goddard Earth Observing System version 4 (GEOS-4) meteorological reanalyses [*Bloom et al*., 2005] to separately drive the model for the year 2005. MERRA is available at 1/2° latitude by 2/3° longitude horizontal resolution with 72 vertical layers (~38 in the tropical troposphere) up to 0.01 hPa. GEOS-4 is available at 1° latitude by 1.25° longitude horizontal resolution with 55 vertical layers (~17 in the troposphere) up to 0.01 hPa. We degraded both products to 2° latitude by 2.5° longitude horizontal resolution for input to GEOS-Chem while maintaining native vertical resolution. We used the Unified Chemical Mechanism (UCX) that fully resolves both tropospheric and stratospheric chemistry [*Eastham et al*., 2014], including online calculation of $O(^3P)$ and $O(^1D)$ chemistry. This mechanism yields modeled O_3 within ±17% of ozonesonde data (±11% in the tropics) when driven by GEOS-5 meteorology. Each simulation was repeatedly cycled over 2004 and 2005 for five iterations, with the first 9 years discarded as initialization.

Base anthropogenic emissions are from the EDGAR v3.2-FT2000 inventory for inorganic compounds [*Olivier et al*., 2005] and from the RETRO inventory for organic compounds [*Schultz et al*., 2007], with regional overwrites for the United States (EPA National Emissions Inventory 2005), Canada (National Pollutant Release Inventory), Mexico [*Kuhns et al*., 2005], Europe [*Auvray and Bey*, 2005], and South and East Asia [*Streets et al*., 2006] and are all scaled to year 2005 on the basis of economic data [*van Donkelaar et al*., 2008]. Separate inventories are used for ammonia [*Bouwman et al*., 1997], black carbon [*Leibensperger et al*., 2012], and ethane [*Xiao et al*., 2008]. Methane is prescribed at the surface to a global mean of 1780 ppbv and allowed to advect and be consumed, with similar treatment of chlorofluorocarbons and other long-lived stratospheric ozone-depleting substances [*Eastham et al*., 2014]. Aircraft emissions are described by *Stettler et al*. [2011] and distributed at altitude along flight corridors. Shipping emissions are described by *Vinken et al*. [2011]. Biomass burning emissions are from the Global Fire Emissions Database version 3 [*van der Werf et al*., 2010]. Biogenic hydrocarbon emissions from terrestrial plants follow the Model of Emissions of Gases and Aerosols from Nature scheme version 2.1 [*Guenther et al*., 2012]. Lightning NO_x emissions are computed online in active deep convection, as described by *Murray et al*. [2012]. Soil microbial NO_x emissions are described by *Hudman et al*. [2012]. In addition to the base 2005 emission simulation, we also perform a preindustrial-like emissions scenario, in which fuel combustion and industrial and agricultural emissions are removed and surface methane is set to 730 ppbv.

Note that GEOS-Chem does not yet have the capability to treat oxygen isotopes and isotopologues explicitly. Explicit treatment imposes a significant computational burden (>300 additional reactions for the O_2 photochemical system alone [*Yeung et al.*, 2014]) and a parameterization for their temporal evolution has not yet been developed. Consequently, the detailed transport histories of O_2 isotopologues are not known, and spatial variations in Δ_{36} are not simulated. Some inferences can be made by comparing simulated isotope equilibration timescales with empirically constrained transport timescales, however. Furthermore, if Δ_{36} is well mixed in the troposphere, quantities integrated over the whole troposphere can be compared to the surface observations using the two-box model described in section 2.2.

We used modeled $O(^3P)$ and O_2 concentrations, known isotope exchange rates (k_{exch}, which are weakly temperature dependent) [*Wiegell et al.*, 1997], temperature (T), air mass (m), and residence times (τ_{box}) in each grid box to calculate the tropospheric rate of isotope exchange (E_{trop}) and the mean temperature at which O_2 isotope exchange occurs in the troposphere ($T_{equil,}$ yielding a corresponding $\Delta_{36,Tequil}$). Unless otherwise specified, we used annual-mean concentrations and temperatures to calculate the quantities described below. Using daytime values yielded identical results at the reported level of precision.

Formally, E_{trop} (mol yr^{-1}) can be defined as the mass- and time-weighted integral of equilibration rates E_V in all tropospheric volumes dV:

$$E_{trop} = \frac{\int_{V_{trop}} E_V\left(\left[O\left(^3P\right)\right], [O_2], k_{exch}(T)\right) m_V \tau_{trop,V} dV}{\int_{V_{trop}} m_V \tau_{trop,V} dV} \times V_{trop} \quad (3)$$

for which $\int V_{trop} dV = V_{trop}$. Equation (3) can be discretized as

$$E_{trop} \approx \frac{\sum_{trop\ grid\ boxes} \left\{k_{exch}(T)\left[O\left(^3P\right)\right][O_2] \times m_{box} \times \tau_{box}\right\}}{\sum_{trop\ grid\ boxes} \left\{m_{box} \times \tau_{box}\right\}} \times V_{trop} \quad (4)$$

$$T_{equil} \approx \frac{\sum_{trop\ grid\ boxes} \left\{k_{exch}(T)\left[O\left(^3P\right)\right][O_2] \times m_{box} \times \tau_{box} \times T_{box}\right\}}{\sum_{trop\ grid\ boxes} \left\{k_{exch}(T)\left[O\left(^3P\right)\right][O_2] \times m_{box} \times \tau_{box}\right\}} \quad (5)$$

The first term in equation (4) represents the mass-weighted mean rate of isotope equilibration in mol m^{-3} yr^{-1}. For the purposes of weighting, residence times in each grid box (allowing for reentry) are assumed to be proportional to the air density at steady state (see the Appendix A). The total volume of the troposphere (V_{trop}) depends on the mean altitude of the tropopause, which varies according to how the tropopause is defined. It was not independently varied in this study but ranges from 4 to 8×10^{18} m^3 for mean tropopause altitudes between 8 km and 15 km. For this study, we use the air mass and density in each grid box, combined with the dynamical tropopause as defined by each meteorological scheme, to calculate the volume of the troposphere. Equation (5) represents the tropospheric T_{equil} resulting from the weighting scheme in equation (3). The whole-troposphere $\Delta_{36,Tequil}$ values were calculated using the theoretical temperature dependence of Δ_{36} at isotopic equilibrium [*Wang et al.*, 2004]. Uncertainties in E_{trop} and T_{equil} arise from the definition of the tropopause, parameterization of transport (residence times for each tropospheric box, in particular), as well as the intrinsic model-dependent uncertainties. A discussion of these uncertainties can be found in the Appendix A.

3. Results

3.1. Measurements of the Present-Day Atmosphere

In the stratosphere, measured Δ_{36} values were typically between 2.5 and 3.0‰, consistent across field campaigns, while Δ_{36} values were between 1.8 and 2.3‰ in the troposphere (Figures 2a and 2c). Elevated Δ_{36} values in the midlatitude lower and middle stratosphere resemble the equilibrium values for the temperatures measured at the time of sampling (Figure 2b). Evidence for elevated Δ_{35} values consistent with isotopic equilibrium was also observed (see Table S1), but the observations were less precise due to lower natural abundances of $^{17}O^{18}O$. The bulk isotopic composition is constant within analytical uncertainties (i.e., $\delta^{18}O$ and $\delta^{17}O$; Table S1), indicating that mesospheric influences are likely negligible [*Thiemens et al.*, 1995; *Liang et al.*, 2007; *Yeung et al.*, 2009].

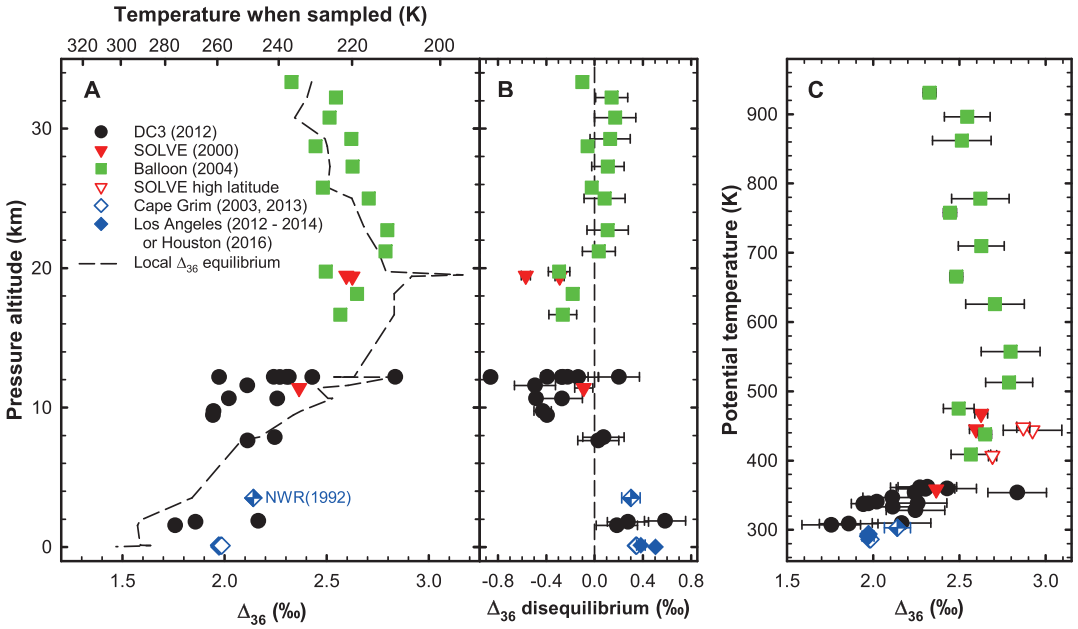

Figure 2. Measured atmospheric Δ_{36} values versus height. Pressure-altitude versus (a) Δ_{36} values and (b) Δ_{36} disequilibrium in the midlatitudes are shown, as well as (c) potential temperature, θ, versus Δ_{36} values for the entire data set. The checkered symbol corresponds to air sampled at Niwot Ridge, Colorado (NWR, 40.05°N, −105.6°W; 3523 m asl) in 1992. Dashed lines show equilibrium Δ_{36} values corresponding to the temperatures at which the air was sampled. Error bars represent 1σ uncertainties, except for surface samples, for which the error bars represent 1 standard error of the mean. Error bars have been omitted from Figure 2a for clarity.

The Δ_{36} values decrease with altitude from ~18 km to the surface ($\theta < 500$ K), across all latitudes and years (Figure 2c). Replicate Δ_{36} measurements at the surface in both hemispheres indicate that surface air is not at isotopic equilibrium with local temperatures (e.g., $p < 5 \times 10^{-9}$ in Houston; Table S1). These observations are consistent with our expectations of rapid isotope reordering in the middle stratosphere and slower isotope reordering in the lower stratosphere and troposphere.

We observe no correlation between Δ_{36} and N_2O above the lowermost stratosphere in the Fort Sumner balloon samples ($r^2 = 0.23$ for $\theta > 380$ K), but a negative correlation for the SOLVE samples ($r^2 = 0.95$; Figure 3a). The former is consistent with an isotope reordering timescale faster than the timescale for mixing in the lower stratosphere (i.e., several months [*Boering et al*., 1996; *Plumb*, 2007]). The latter may be related to the altitudes from which they were sampled: both the Fort Sumner balloon samples and SOLVE samples from 16 to 20 km (400 K $< \theta <$ 500 K) are in isotopic disequilibrium to a similar degree (Figure 2b). If the isotope exchange rates in the lower stratosphere are sufficiently slow compared to timescales of mixing, isotopic disequilibrium would be expected because the Δ_{36} values of these samples would represent isotopic exchange reactions integrated along their transport pathway, thus bearing little resemblance to the temperatures at time of sampling except by coincidence. Yet the short timescales of isotope equilibration in that region may be too short for the observed correlation to represent a global "slope equilibrium" [after *Plumb and Ko*, 1992] that could be used to derive a net isotope flux between stratosphere and troposphere. Additional measurements on similar samples may address the generality of this correlation in the lower troposphere and its potential utility for constraining STE fluxes of Δ_{36}.

The Δ_{36} values for samples taken during a nearly isentropic and isothermal (within 3 K) flight across the tropopause indicate that mixing strongly modulates Δ_{36} values near the tropopause (Figure 3b). The timescales of isentropic transport are equal to or shorter than the timescales for isotopic equilibration in that region ($\tau_{\text{equilibration}}$ ~ months versus transport within weeks [*Boering et al*., 1996]), so the samples likely represent mixtures of air from different regions. A 0.9‰ range was observed during the initial tropopause crossing when a 0.3‰ range would be expected based on temperatures alone (Figure 3b). Similarly elevated Δ_{36} values were observed for some samples obtained from the upper troposphere, where intrusions of

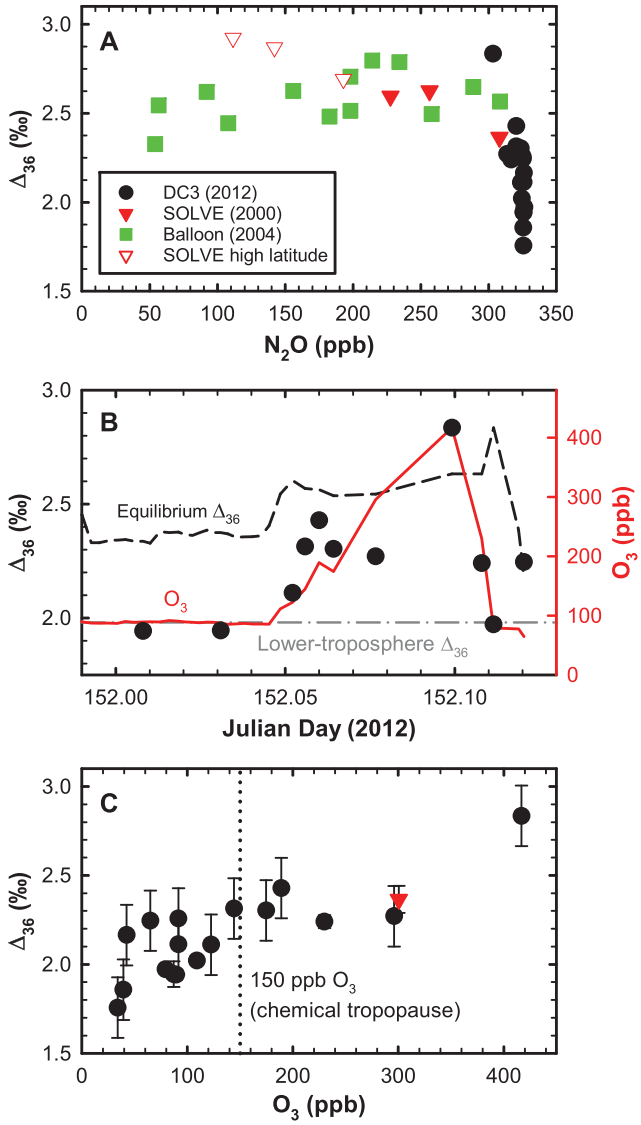

Figure 3. Comparison of atmospheric Δ_{36} values with other tracers. (a) Δ_{36} values plotted against N_2O. A correlation implies that timescales of O_2 isotope reordering are longer than those of mass transport. The correlation observed for SOLVE samples requires more data to verify (see section 3.1). (b) Measured Δ_{36} values for a cross-tropopause flight during the DC3 campaign, plotted with O_3 concentrations and Δ_{36} values for local isotopic equilibrium. (c) Measured Δ_{36} versus O_3 near the 150 ppb chemical tropopause. Note the data from the SOLVE mission (red triangle; mean ± 1σ, $n = 3$), which is consistent with the DC3 data despite the 12 year difference in sampling date. Error bars have been omitted from Figures 3a and 3b for clarity.

stratospheric air masses often occur [*Stohl et al.*, 2003; *Škerlak et al.*, 2014]. Tropospheric air from 8 to 12 km ($\theta \approx 330$–350 K) sampled during the DC3 campaign was up to 0.3‰ higher in Δ_{36} than in surface air (Figures 2 and 3). Air sampled from Niwot Ridge, CO (3523 m above sea level (asl)) in 1992, also has a Δ_{36} value 0.15 ± 0.08‰ (1σ) higher than air sampled from Cape Grim that same year (94 m asl; Figure 2a and Table S1). These variations may be episodic, as not all upper troposphere samples had elevated Δ_{36} values. Many of the DC3 samples were sampled in deep convective midlatitude storms that are associated with STE, and Niwot Ridge is influenced by periodic stratosphere-to-troposphere transport (STT) of air [*Pan et al.*, 2014; *Schroeder et al.*, 2014; *Sullivan et al.*, 2015]. Some Δ_{36} values nevertheless appear close to local isotopic equilibrium (Figure 2b). These agreements are probably coincidental, as air mass residence times in this region are far shorter than expected local isotope equilibration timescales ($\tau_{\text{equilibration}} > 1$ year).

Table 1. Δ_{36} Values Measured in Archived Surface Air

Sample	Date(s)	Latitude (°N)	Longitude (°W)	$\Delta_{36} \pm 1$ SE (‰)	*n*
Houston	2016	29.76	95.37	1.972 ± 0.011	17
Los Angeles[a]	2012–2014	34.07	118.44	1.97 ± 0.03	23
Cape Grim (G050-211)	7/5/2013	−40.68	−144.69	1.978 ± 0.011	3
Cape Grim (G050-209)	2/17/2003	−40.68	−144.69	1.985 ± 0.017	3
Cape Grim (G050-208)	9/23/1992	−40.68	−144.69	1.963 ± 0.020	3
Cape Grim (G050-207)	2/6/1986	−40.68	−144.69	1.978 ± 0.024	3
Cape Grim (G050-206)	4/26/1978	−40.68	−144.69	1.974 ± 0.027	3

[a]From *Yeung et al.* [2014].

The mean of air measurements in Los Angeles ($\Delta_{36} = 1.97 \pm 0.03$‰, 1 SE), Houston ($\Delta_{36} = 1.972 \pm 0.011$‰, 1 SE), and Cape Grim (e.g., $\Delta_{36} = 1.978 \pm 0.011$‰ in 2013, 1 SE; see Table 1) were indistinguishable within analytical uncertainties. Furthermore, Δ_{36} values from 1 to 2 km, sampled during DC3 ($\Delta_{36} = 1.93 \pm 0.12$‰; 1 SE, analyzed at UCLA), are also similar to surface Δ_{36} values. This close correspondence in Δ_{36} between Northern and Southern Hemisphere sites, including one from a high-O_3 region (Los Angeles basin) and one from a low-O_3 region (Cape Grim), suggests that surface Δ_{36} values are insensitive to the local differences in photochemistry set by abundances of nitrogen oxide radicals and volatile organic compounds. Moreover, surface Δ_{36} values are not at isotopic equilibrium with their surroundings, and they are too low to be stratospheric in origin (where $\Delta_{36} \geq 2.3$‰). They must reflect O_3 photochemistry taking place elsewhere in the troposphere. We suggest that mean Δ_{36} values at the surface reflect O_3 photochemistry integrated at least hemispherically, if not throughout the whole troposphere: Rapid tropospheric stirring [*Wofsy*, 2011; *Waugh et al.*, 2013] will lead to a narrow distribution of Δ_{36} values at the surface if isotopic equilibration is slower than the ~1 year mixing timescale of the troposphere. Intrusions of stratospheric air into the lower troposphere may cause short-term variability in Δ_{36} values at the surface, but mean Δ_{36} values within ±0.01‰ in both hemispheres indicate that, at least on annual timescales, local influences on the clumped-isotope distribution of O_2 at the surface are negligible.

3.2. Comparison of Present-Day Measurements With GEOS-Chem Model Results

We ran chemical transport simulations of the atmosphere for the present-day atmosphere using the GEOS-Chem atmospheric chemistry model forced by either the MERRA or GEOS-4 meteorological reanalyses for the year 2005. Both model implementations show that O_3 and $O(^3P)$ covary throughout the atmosphere because of rapid O_3 photolysis and recombination (Figures 5a–5d). Photolysis of nitrogen dioxide (NO_2), although important in polluted air masses in the northern midlatitudes, has a much smaller effect on tropospheric atomic oxygen in the rest of the atmosphere, contributing <2% to tropospheric $O(^3P)$ production (Figures 5e and 5f; note the difference in scale relative to Figures 5c and 5d).

At >20 km altitude, our model and several others [e.g., *Brasseur et al.*, 1990] predict that timescales of isotope equilibration are several days or less. Generally, our observations in this region are consistent with these model results, as the air in that region appears to be near isotopic equilibrium with local temperatures (Figure 2b). The disequilibria observed between 16 km and 20 km altitude noted in section 3.1 also do not seem unreasonable given the timescales of isotope equilibration there (Figure 4): equilibration takes a week to a month, comparable to the timescales for horizontal transport in this region (<1 month [*Boering et al.*, 1996]). As noted previously by others [*Boering et al.*, 1996; *Mote et al.*, 1996; *Schoeberl et al.*, 2006], a significant fraction of the air in the lower stratosphere has only recently entered the stratosphere, so we hypothesize that it has not yet been fully reequilibrated at stratospheric temperatures.

We calculated a whole-troposphere isotopic equilibration rate of $E_{trop} = 1.3 \times 10^{19}$ mol O_2 yr^{-1} using modeled isotope exchange rates, air masses, and air density in each grid box (see section 2.3 and Appendix A). About one half to one third of the tropospheric O_2 inventory (3×10^{19} mol O_2) undergoes isotope exchange annually. This tropospheric rate of isotope reordering is ~400 times faster than biological O_2 cycling [*Blunier et al.*, 2012] and similar to that of whole-troposphere tracer mixing [*Waugh et al.*, 2013]. It justifies our treatment of the troposphere as a geochemical box within which Δ_{36} values are driven toward an equilibrium end-member, $\Delta_{36,Tequil}$, by photochemistry on annual timescales. This end-member can be calculated

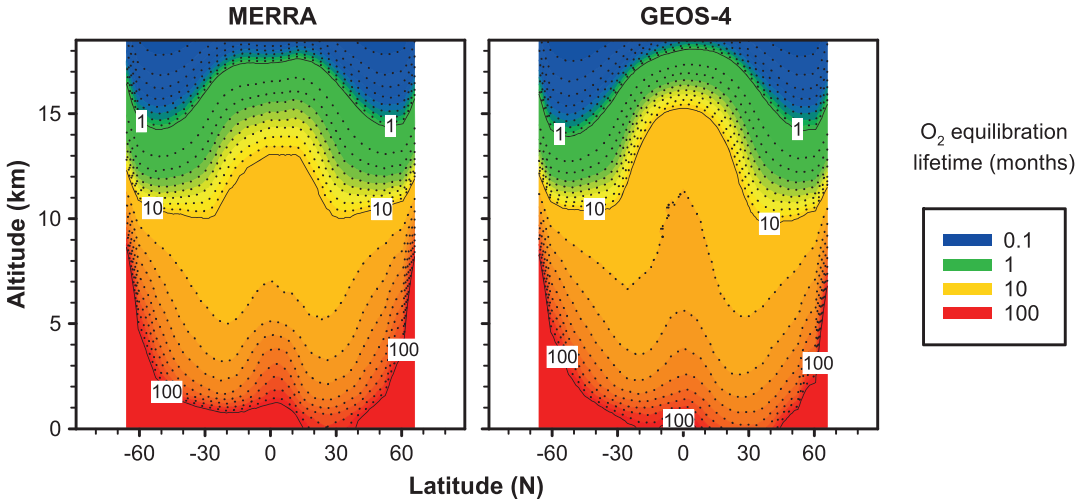

Figure 4. Calculated zonal-mean O_2 equilibration lifetimes in the troposphere and lower stratosphere. Labeled and colored contours depict the lifetimes, i.e., $\tau = (k_{exch} \times [O(^3P)])^{-1}$, expressed in months, shown on a logarithmic scale. Equilibration lifetimes for polar latitudes are not shown; they are exceedingly long because negligible atomic oxygen is produced there during polar night.

using annually averaged spatial distributions of O_3 (via atomic oxygen), temperature, air mass in each grid box, and air density (a proxy for residence time; see section 2.3).

The calculated whole-troposphere equilibrium end-members are $\Delta_{36,Tequil} = 1.93‰$ for MERRA and 1.90‰ for GEOS-4 meteorology in 2005. Isotopic reordering in the subtropical free troposphere (4–6 km) contributes the most to the weighting of $\Delta_{36,Tequil}$ values (Figures 5 and 6). The spatial weighting patterns for MERRA and GEOS-4 are similar, but the maxima are at higher altitudes in MERRA, perhaps reflecting its weaker vertical fluxes of low-O_3 air from the marine boundary layer into the upper troposphere [*Liu et al.*, 2010]. For example, at 215 hPa (~11 km), the vertical velocities in the MERRA meteorology are about a factor of 2 lower than in GEOS-4 [*Liu et al.*, 2013b]. A larger proportion of tropospheric O_3 photochemistry occurs in the upper troposphere in MERRA/GEOS-Chem simulations as a result (Figures 5a and 5b), yielding a higher whole-troposphere $\Delta_{36,Tequil}$ value. Slightly higher cloud top heights in the MERRA meteorology [*Murray et al.*, 2012] may also contribute to the differences in calculated whole-troposphere $\Delta_{36,Tequil}$ values.

There is a notable minimum of weighting within the intertropical convergence zone in both meteorologies, and seasonal patterns that imply a connection between $\Delta_{36,Tequil}$ values and global circulation (i.e., the Hadley, Walker, and Brewer-Dobson circulations; Figure 6). In particular, the altitudes and latitudes of the $\Delta_{36,Tequil}$ weighting maxima suggest that $\Delta_{36,Tequil}$ is associated with the descending branches of the tropical overturning circulations. Patterns of STT of O_3 are also visible in the extratropics, e.g., a maximum in STT O_3 flux in the late spring and summer in the Northern Hemisphere [*Škerlak et al.*, 2014]. Generally, climatological patterns of O_3 resemble the patterns in Figure 6 [*Liu et al.*, 2013a], supporting a link between O_3, tropical circulation, and tropospheric Δ_{36} values.

Previous studies have associated subtropical O_3 variability with the 30–90 day Madden-Julian Oscillation [*Ziemke and Chandra*, 2003b] as well as the interannual El Niño–Southern Oscillation [*Ziemke and Chandra*, 2003a] in the tropical Pacific, the origins of which stem from a combination of O_3 transport, changing precursor emissions from biomass burning, and lightning [*Sudo and Takahashi*, 2001; *Tian et al.*, 2007; *Murray et al.*, 2013; *Sun et al.*, 2014; *Virts and Wallace*, 2014; *Ziemke et al.*, 2015]. Other transport mechanisms important in these regions include horizontal mixing between tropical and extratropical air masses and downward transport of O_3 from the stratosphere [*Waugh and Polvani*, 2000; *Hsu et al.*, 2005; *Neu et al.*, 2014]. The relative importance of these mechanisms is beyond the scope of this report, but we assert that the whole-troposphere $\Delta_{36,Tequil}$ value is sensitive to tropical meteorology via the factors that control O_3 in the troposphere.

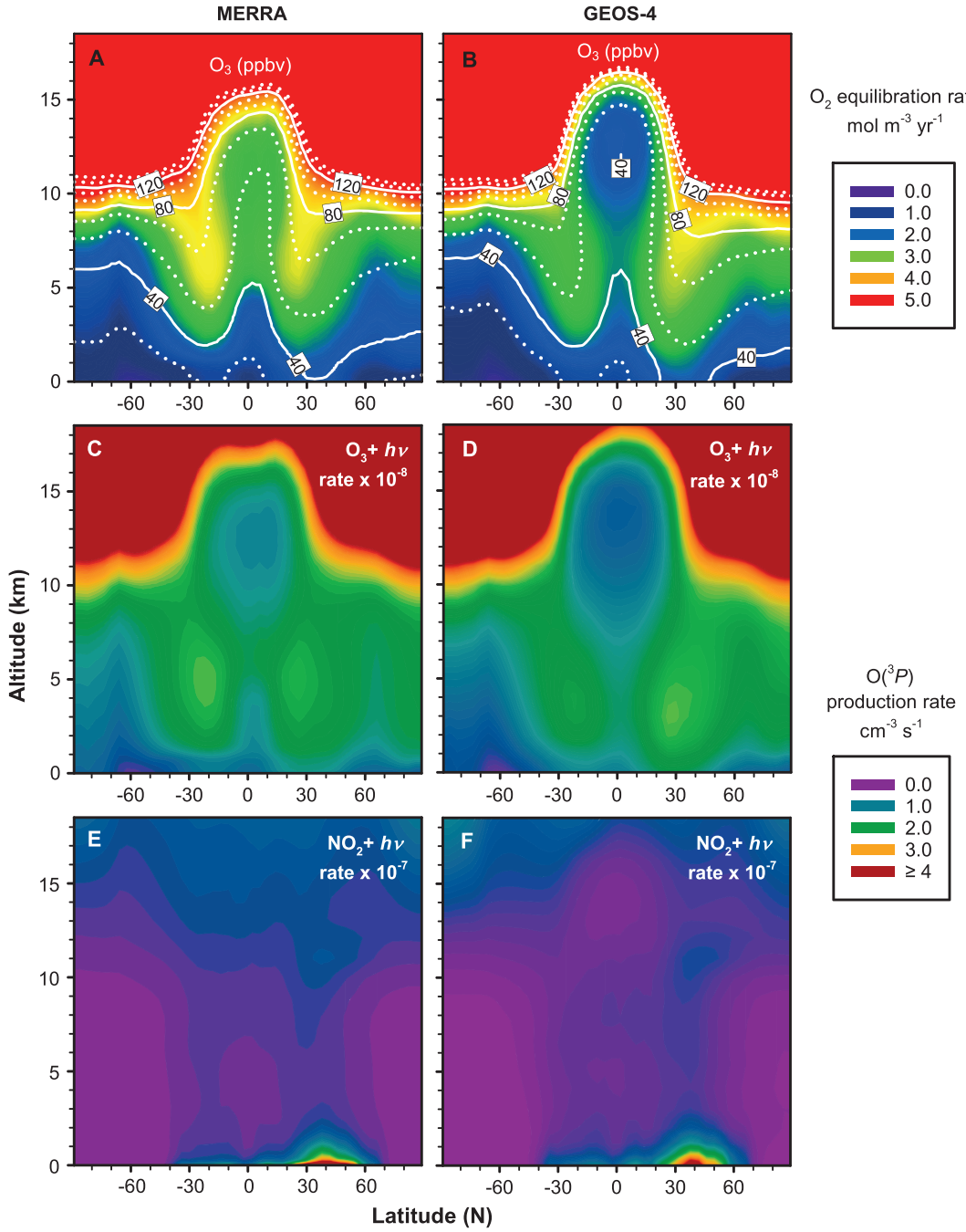

Figure 5. Correspondence between O_3, $O(^3P)$, and rates of O_2 isotope equilibration. Left and right columns show annually averaged zonal-mean results from GEOS-Chem simulations (year 2005) using MERRA and GEOS-4 meteorologies, respectively. (a and b) O_3 concentrations (ppbv; white contours) overlain atop isotope equilibration rates (mol m^{-3} yr^{-1}; colored contours). (c and d) show the strength of the O_3-photolysis source of $O(^3P)$; (e and f) the strength of the NO_2 photolysis source of $O(^3P)$. Note the order-of-magnitude difference in scales for $O(^3P)$ production rate shown on the plots.

For example, convective and advective transport of O_3-poor air from the surface to the upper troposphere, mainly in the intertropical convergence zone, reduces the amount of tropospheric O_3 at high tropical altitudes (e.g., Figures 5a and 5b). Subsequent entrainment of O_3-rich air from the upper troposphere during subsidence increases O_3 at midtropospheric altitudes of the subtropics. These large-scale circulation patterns reduce O_2 isotope exchange rates in the coldest regions of the tropics and enhance O_2 isotope exchange

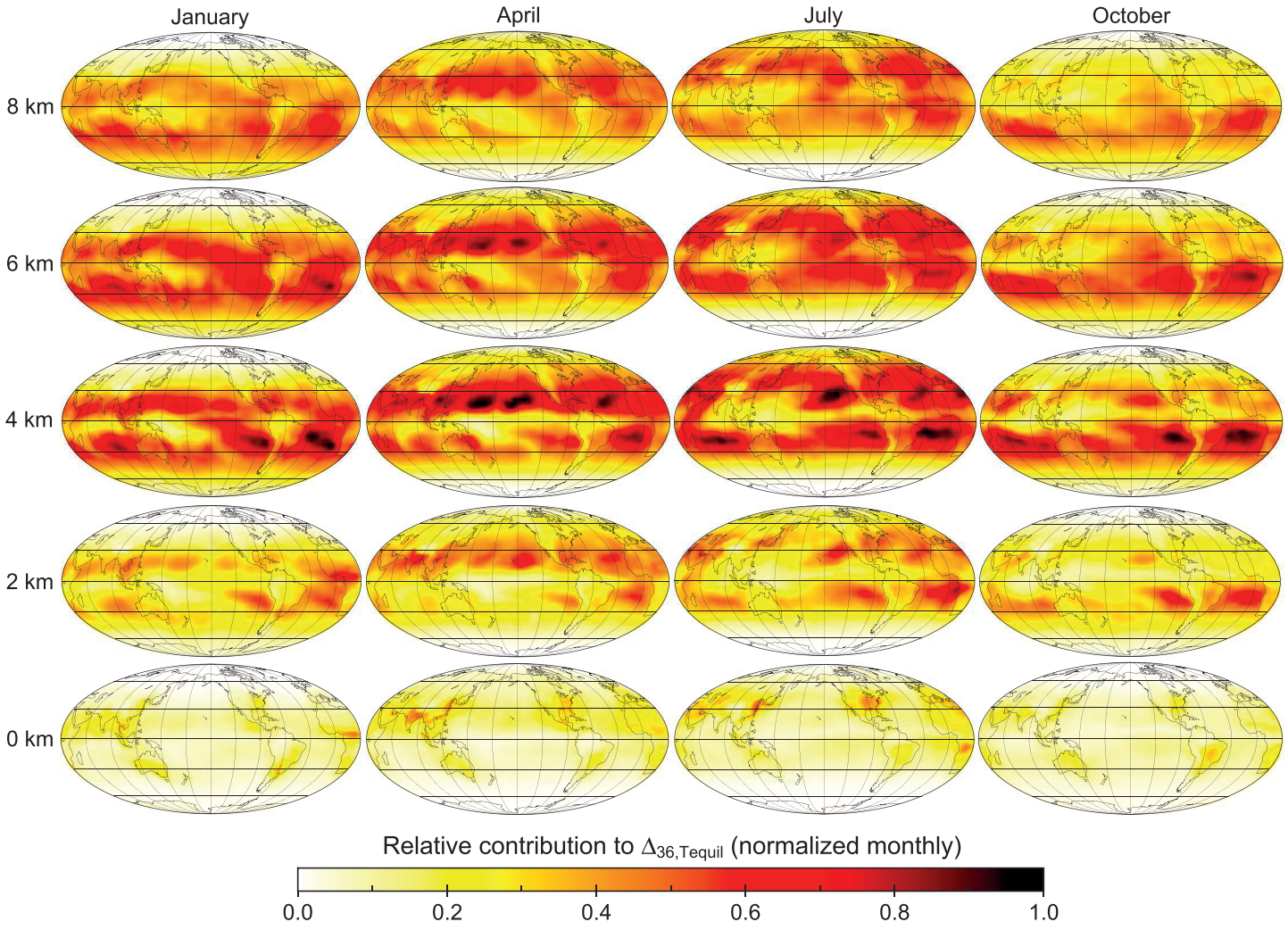

Figure 6. Spatial and temporal patterns of isotope reordering derived from GEOS-Chem/MERRA simulations. The maps shown highlight the regions where O_2 isotope reordering occurs during model year 2005. Darker colors indicate a larger contribution to the whole-troposphere $\Delta_{36,Tequil}$ value. Similar results were obtained for GEOS-4 simulations.

rates in warmer regions (Figures 5c, 5d, and 6). Therefore, the Hadley circulation acts to decrease the whole-troposphere $\Delta_{36,Tequil}$ value relative to a scenario in which O_3 is uniformly distributed with altitude. Changes in the vertical extent, mass flux, and entrainment that characterize this circulation may affect the whole-troposphere $\Delta_{36,Tequil}$ value through its effects on O_3 transport and photochemistry [*Wu et al.*, 2007].

The present-day timescale of isotope equilibration in the troposphere (2–3 years) is longer than the timescale of whole-troposphere mixing (~1 year), so spatial variations in Δ_{36} values are expected to be small. Indeed, the observational dataset presented in section 3.1 shows no statistically significant tropospheric Δ_{36} variations outside of regions with known stratosphere-troposphere mixing. Therefore, we restrict further measurement-model comparison to quantities that integrate O_3 photochemistry on annual timescales—surface Δ_{36} values and whole-troposphere $\Delta_{36,Tequil}$ values—which should be robust in both the measurements and the model.

Mean Δ_{36} values measured at the surface (e.g., 1.972 ± 0.011‰ in Houston; 1 SE) are similar to calculated whole-troposphere $\Delta_{36,Tequil}$ values, but slightly higher. We infer that isotopic ordering in O_2 at the surface is nearly equilibrated to the whole-troposphere $\Delta_{36,Tequil}$ end-member despite the large flux of high-Δ_{36} air entering the troposphere (STT mass flux $= 4.6 \times 10^{18}$ mol O_2 yr^{-1}). The stratospheric contributions implied by isotopic mass balance are consistent with the mixing fractions implied by the shorter-lived ^{7}Be tracer of

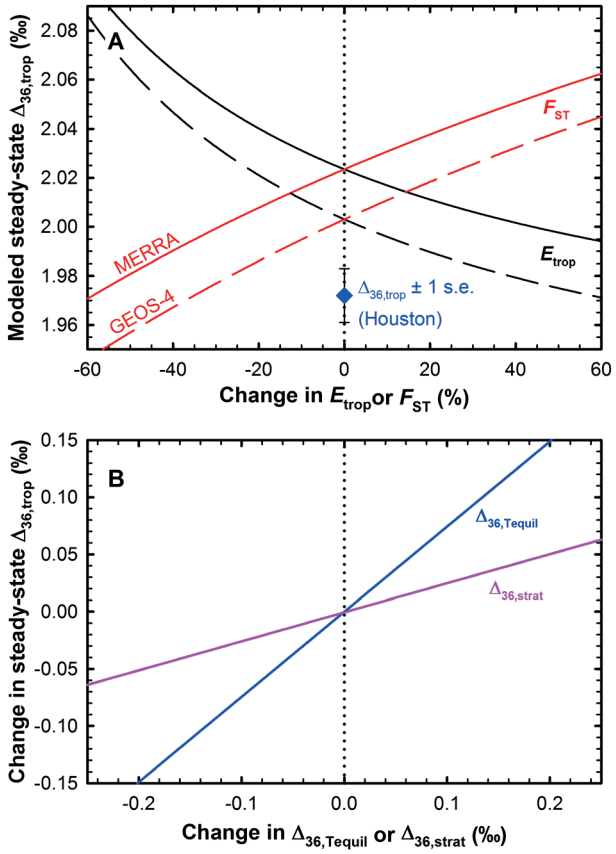

Figure 7. Sensitivity tests of the two-box atmospheric model. Shown is the dependence of the $\Delta_{36,trop}$ value on (a) STT mass flux (F_{ST}) and whole-troposphere isotope equilibration rate (E_{trop}) or (b) the whole-troposphere $\Delta_{36,Tequil}$ value and the $\Delta_{36,strat}$ value, keeping all else constant. Two-box model results using both the MERRA and GEOS-4-derived end-members are shown in Figure 7a.

STT (20–30% stratospheric in the northern midlatitudes [*Murray et al.*, 2014]). Furthermore, using these stratospheric and tropospheric end-members in our two-box model yields a mean tropospheric $\Delta_{36,trop}$ value similar to the observations at steady state, although slightly higher (2.02‰ and 2.00‰ for MERRA and GEOS-4, respectively; these estimates include the effects of biosphere O_2 cycling).

Some uncertainty in these two-box model estimates arises from uncertainties in the kinetic rates of O_2 isotope exchange in the atmosphere, however. The experimental uncertainty in the magnitude of k_{exch} (the O_2 isotope exchange rate coefficient) ±30% (2σ) [*Wiegell et al.*, 1997], affects E_{trop} values, while the uncertainty in its temperature dependence affects $\Delta_{36,Tequil}$ values. The former contributes $^{+0.03}_{-0.02}$‰, while the latter contributes less than ±0.01‰ uncertainty to our steady state $\Delta_{36,trop}$ estimates, yielding a combined uncertainty of $^{+0.03}_{-0.02}$‰ (2σ). Consequently, the $\Delta_{36,trop}$ estimate derived from the GEOS-4 meteorology appears consistent with the surface Δ_{36} measurements, while the MERRA meteorology may be slightly too high, if these are the major sources of systematic error in the tropospheric term within equations (1) and (2). We note that several independent estimates of k_{exch} near 300 K agree within 10% [*Anderson et al.*, 1985; *Wiegell et al.*, 1997], suggesting that the uncertainty limits reported here are conservative.

Sensitivity tests within the two-box model framework indicate that the steady state $\Delta_{36,trop}$ value is not strongly forced by STT of O_2 (Figure 7); it is instead controlled by tropospheric factors, specifically the whole-troposphere $\Delta_{36,Tequil}$ value. Changes in the tropospheric steady state $\Delta_{36,trop}$ value of order 0.01‰ require variations of about 15% in F_{ST} or 0.04‰ in $\Delta_{36,strat}$ value (Figures 7a and 7b). Interannual variations in STT mass flux are only large enough to perturb $\Delta_{36,trop}$ by ~0.001‰ [*Škerlak et al.*, 2014]. In addition, a large error in $\Delta_{36,strat}$ value is unlikely given our observational constraints (Figures 2 and 3) and the insensitivity of steady state $\Delta_{36,trop}$ value to tropopause definition (see Appendix A). Consequently, a change in $\Delta_{36,trop}$ value forced by the stratospheric transport term would only occur under extraordinary circumstances. In contrast, a change in $\Delta_{36,trop}$ value forced by the tropospheric term is plausible: the tropospheric equilibration rate, E_{trop}, which is three times larger than F_{ST} in the present day, dominates the tropospheric Δ_{36} budget. Furthermore, because tropospheric O_2 is nearly equilibrated to the whole-troposphere $\Delta_{36,Tequil}$ value, the $\Delta_{36,trop}$ value is most sensitive to the assumed whole-troposphere $\Delta_{36,Tequil}$ value in our two-box model (Figure 7b). In general, F_{ST} and E_{trop} oppose each other in equation (2), so a decrease in E_{trop} would result in an increased sensitivity of $\Delta_{36,trop}$ to the stratospheric terms of the Δ_{36} budget and vice versa.

We note that the similarity between whole-troposphere $\Delta_{36,Tequil}$ values and measured surface Δ_{36} values implies that O_2 at the surface has resided in the troposphere for at least 4 years, on average. More precisely, it has not experienced significant photochemical reordering in the stratosphere during that time. Recent

simulations suggest that one third to one half of air parcel trajectories entering the stratosphere in the tropics return to the troposphere in less than 3 months [*Orbe et al*., 2014]; if these trajectories tend to remain within the lowermost stratosphere where O_2 reordering timescales are slow (Figure 4), then the air will still be largely "tropospheric" in its Δ_{36} value when it exits the stratosphere. We conclude that the surface Δ_{36} value is controlled by the whole-troposphere $\Delta_{36,Tequil}$ value and forced weakly by stratospheric factors.

3.3. Archived Air From 1978 to 2013: A Sensitivity Test for Tropospheric Δ_{36} Values

To investigate the sensitivity of tropospheric Δ_{36} values to global changes in atmospheric properties during the twentieth century, we analyzed air samples from the Cape Grim air archive dating back to 1978 [*Langenfelds et al*., 1996]. Historical ozonesonde measurements indicate that O_3 has increased throughout the troposphere since 1978, by up to 30% at some sites [*Logan et al*., 2012; *Cooper et al*., 2014]. Meanwhile, changes in STE mass flux have been observationally constrained to be $<$10% [*Butchart et al*., 2006; *Škerlak et al*., 2014]. Tropopause temperatures have changed less than 2°C [*Seidel et al*., 2001; *Santer et al*., 2003], so changes in $\Delta_{36,strat}$ have a negligible impact on the tropospheric budget. Moreover, tropospheric temperature structure has been relatively constant amidst a global ~1 K warming [*Santer et al*., 2013]. Finally, a recent global satellite-based time series analysis found that cloud top heights (a proxy for the vertical extent of tropical circulation relevant to $\Delta_{36,Tequil}$) had a long-term trend of $\leq 2\,m\,yr^{-1}$ between 1996 and 2011 [*Lelli et al*., 2014], too small to be detectable by Δ_{36}, even when extrapolated back to 1978. The most important atmospheric trend from 1978 to 2013 for surface Δ_{36} values was therefore that of an increasing tropospheric O_3 burden. If the two-box model is an adequate description of the global budget, then one would expect surface Δ_{36} values to decrease as the total tropospheric O_3 burden increases. An anthropogenic increase in O_3 near the surface would decrease $\Delta_{36,Tequil}$ and therefore also surface Δ_{36} values over this time period.

We find that Δ_{36} values in the archived air samples are all indistinguishable, with mean values within 0.01‰ of recent surface values (see Table 1). We infer that changes in anthropogenic O_3 at the surface since 1978 were smaller than the current limit of detection by Δ_{36} values. Holding all else equal, a surface Δ_{36} value constant within ±0.01‰ over this time period would imply that the tropospheric O_3 burden has stayed within a ~ ±10% range since 1978. This result agrees with the 5% increase in the tropospheric O_3 burden since 1980 predicted by the Atmospheric Chemistry-Climate Modeling Intercomparison Project (ACCMIP ensemble mean) [*Young et al*., 2013]. A more precise measurement-model comparison will require both a higher-precision time series and the inclusion of isotopologue-specific chemistry and transport in the 3-D atmospheric model.

To examine the sensitivity of surface Δ_{36} values to anthropogenic O_3 more generally, we ran a GEOS-Chem simulation using the 2005 MERRA meteorology with preindustrial (i.e., 1850 Common Era) nonfire anthropogenic emissions and methane concentrations of 730 ppb. We obtained a $\Delta_{36,Tequil}$ value for this extreme case, which we input into our two-box model. In that simulation, the largest decreases in O_3 are found at the surface, which leads to a greater proportion of O_3 photochemistry occurring in the middle and upper troposphere. This redistribution of O_3 photochemistry, away from the warm surface and toward the colder free troposphere, results in a $\Delta_{36,Tequil}$ value that is higher by 0.02‰. The overall tropospheric O_3 burden is 29% lower (256 Tg O_3 versus 362 Tg O_3), and tropospheric rates of O_2 reordering are reduced by 37% ($E_{trop} = 8.4 \times 10^{18}$ mol O_2 yr^{-1} versus 1.3×10^{19} mol O_2 yr^{-1}). Consequently, STT is a more important component in the tropospheric Δ_{36} budget (i.e., the $F_{ST}\Delta_{36,strat}$ term in equation (2)), leading to an additional increase of $\Delta_{36,trop}$ values. The model therefore predicts that these preindustrial $\Delta_{36,trop}$ values are ~0.05‰ higher than in the present day, all else being equal. Further sensitivity tests indicate that surface Δ_{36} values are still insensitive to variations in STT mass flux at these reduced E_{trop} values: an unprecedented 25% increase in F_{ST} would be required to increase $\Delta_{36,trop}$ by 0.02‰.

While O_3 trends since 1978 may not have been detectable in the surface Δ_{36} value, the preindustrial-to-industrial increase in O_3 may be observable in ice-core air archives with modest improvements in analytical precision. It is currently limited only by counting statistics and thermal (Johnson) noise on the Rice University instrument, so extending integration times and/or increasing the size of ion currents should yield the factor of 1.5–2 necessary to quantify the anthropogenic decrease in $\Delta_{36,trop}$ values with high confidence. Note that the $\Delta_{36,trop}$ value is a proxy for the tropospheric O_3 burden rather than a direct measure of it; however, forward atmospheric modeling can relate changes in $\Delta_{36,trop}$ value to changes in atmospheric O_3 burden.

4. Summary and Discussion

What atmospheric properties do tropospheric Δ_{36} values record? It depends on the timescale of interest. In the upper troposphere and lower stratosphere, Δ_{36} values reflect the mass flux between the stratosphere and troposphere on timescales of weeks to months. In the upper troposphere, STT varies the proportion of unaltered "stratospheric" air, which elevates Δ_{36} values above mean values characteristic of the surface. In the lower stratosphere, STE of O_2 lowers Δ_{36} values from that expected at local isotopic equilibrium. These perturbations can be used as air mass mixing tracers on timescales of up to a year and may be useful in diagnosing STE within a Lagrangian framework. In the lower troposphere, Δ_{36} values record quantities related to the concentration and spatial patterns of tropospheric O_3.

To first order, the $\Delta_{36,trop}$ value is an expression of the temperature of the tropical troposphere. The majority of tropospheric O_2 isotope reordering occurs in the subtropics at 4–6 km (Figures 5 and 6), where clear-sky subsidence promotes photochemical O_3 cycling. Stronger convection or advection can decrease upper troposphere O_3 by upwelling more low-O_3 air from the boundary layer (e.g., in GEOS-4, Figure 5b), which causes a larger proportion of O_3 photochemistry to occur at warmer temperatures (Figure 5d). Weaker convection/advection has the opposite effect because the upper troposphere will have more O_3 on average (e.g., MERRA, Figure 5a). The former tends to decrease $\Delta_{36,Tequil}$ and $\Delta_{36,trop}$ values, while the latter tends to increase them, relative to isotopic equilibrium at a fixed midtropospheric temperature.

The difference between the two-box-modeled $\Delta_{36,trop}$ value and the mean Δ_{36} value measured at the surface may thus constitute an additional benchmark for model parameterizations of vertical transport in the tropical troposphere. The present result, with the MERRA meteorology yielding tropospheric $\Delta_{36,trop}$ values that are slightly too high (2.02‰ modeled versus 1.97‰ measured), implies that the transport from the boundary layer into the upper troposphere is too weak in the MERRA meteorology; it is consistent with previous work that found that convection detrains at too low an altitude in the tropical upper troposphere in GEOS-5, a nearly identical meteorology. In contrast, the GEOS-4 meteorology better reproduces tropical tropospheric trace gases during convective events [*Liu et al*., 2010; *Mitovski et al*., 2012] and also shows better agreement with measured Δ_{36} values.

While the STT mass flux is an important part of the atmospheric Δ_{36} budget, our sensitivity tests indicate that its variations only perturb $\Delta_{36,trop}$ values in extraordinary cases. Extreme changes in annually averaged STT mass flux of order several tens of percent or more are required to alter mean Δ_{36} values at the surface significantly. Similarly, variations in the tropospheric O_3 burden of ~10% (which affect E_{trop} values) are near the current limits of detection by Δ_{36} values.

Our model predicts that Δ_{36} values decreased in response to increasing ground-level O_3 sources during the industrial era. Increasing surface O_3 concentrations leads to a greater proportion of O_3 photochemistry occurring at low altitudes (i.e., warmer temperatures), which lowers $\Delta_{36,trop}$ values independent of the circulation. The timing and magnitude of changes in Δ_{36} values over the past century might therefore constrain the increase in tropospheric O_3 burden, which is presently uncertain. Early measurements of ground-level O_3 suggest that it has increased by a factor of 2–3 since the late nineteenth century, but atmospheric models have struggled to reproduce such a strong O_3 increase [*Wang and Jacob*, 1998; *Stevenson et al*., 2013; *Young et al*., 2013; *Cooper et al*., 2014]. The Δ_{36} tracer may be able to distinguish the twentieth century increase in tropospheric O_3 burden increase predicted by models (resulting in a Δ_{36} decrease of –0.05‰ in MERRA) from that implied by historical measurements at the surface (–0.1‰ in Δ_{36} [*Volz and Kley*, 1988; *Marenco et al*., 1994]). The unknown temporal evolution of circulation and STT mass flux over this time period prevents a more rigorous estimate of the atmospheric Δ_{36} evolution at present, but recent work suggests that STT has been either constant or decreasing slightly during the second half of the twentieth century [*Škerlak et al*., 2014; *Oberländer-Hayn et al*., 2016]; thus, the sign and magnitude of the twentieth century Δ_{36} decrease should be robust. The analytical precision required to provide an unequivocal constraint (i.e., better than ±0.02 in Δ_{36}) is likely within the capabilities of current instrumentation.

On longer timescales, the Δ_{36} tracer is sensitive to climatic boundary conditions. For example, lower sea surface temperatures during the last glacial maximum [*MARGO Project Members*, 2009] cool and steepen the lapse rate that characterizes the tropical atmosphere. A cooling of order 10 K in the midtroposphere

has been inferred [*Thompson et al*., 1995; *Stansell et al*., 2007; *Tripati et al*., 2014], which would yield a Δ_{36} value about +0.15‰ higher than its mean Holocene values, all else being equal. Significant deviations from this expected value may indicate a shift in hydrologic, dynamical, or chemical properties of the atmosphere influencing tropical lapse rates and/or the global distribution of O_3. Future modeling studies can test the sensitivity of $\Delta_{36,trop}$ values to climate-driven changes in tropopause height and O_3, which are also relevant. Once the governing boundary conditions can be constrained, the Δ_{36} tracer may shed light on past changes in the structure of the ancient atmosphere. The Δ_{36} tracer can complement more well-known atmospheric temperature proxies such as δD or $\delta^{18}O$ values of precipitation applied in tropical ice-core records [*Thompson et al*., 1995] because (1) its equilibrium values are constrained by quantum-mechanical theory and (2) it integrates atmospheric temperature and dynamics across the entire tropics. Importantly, the subdecadal timescale of tropospheric O_2 isotope reordering could in principle be used as a high-resolution stratigraphic marker for synchronization of atmospheric composition and tropical climate using gases extracted from well-preserved polar ice cores.

The measurements and modeling can be improved in several respects to facilitate these applications. First, tighter constraints on the magnitude and temperature dependence of the $O(^3P) + O_2$ isotope exchange rate coefficient will reduce uncertainties in E_{trop} and $\Delta_{36,Tequil}$ values for all model implementations. Second, grid-scale online calculation of atmospheric Δ_{36} values may reveal subtle spatial variations that will be relevant when comparing model outputs and ice-core Δ_{36} records obtained from high-latitude sites. Third, improvements in the control of photochemical calibration temperatures, combined with increased measurement precision arising from longer integration times, may enable Δ_{36} analyses with an accuracy of 0.01‰ to 0.02‰ (i.e., ~1 K at isotopic equilibrium). If clumped-isotope signatures in O_2 are preserved in paleoatmospheric records, Δ_{36} values could light a path toward understanding how the tropical troposphere evolved during the Pleistocene.

Appendix A: Uncertainties in Calculations for Global Rate of Isotope Equilibration and Whole-Troposphere $\Delta_{36,Tequil}$

A1. Definitions of Tropopause Height

Some uncertainty remains for defining the effective height of the tropopause for the budgets of trace gases. Measurements of CO_2 at the tropical tropopause layer suggest that the upper boundary of the well-mixed troposphere is $\theta = 360$ K in the tropics [*Park et al*., 2007], whereas tracer-tracer studies suggest that the lapse rate tropopause represents the upper boundary in the extratropics [*Pan et al*., 2004]. However, because the lapse rate tropopause may not be unique near the subtropical jet, dynamical tropopause definitions (e.g., troposphere <2 potential vorticity unit) have also been used because it is better represents diabatic flow. Finally, an O_3 concentration is sometimes employed as a threshold for the tropopause when calculating tropospheric burdens, such as $O_3 < 150$ ppb for the troposphere in the Atmospheric Chemistry and Climate Model Intercomparison Project (ACCMIP) [*Young et al*., 2013]. We found that E_{trop} was generally insensitive to tropopause definition: Values derived from tropopause thresholds of 100–150 ppb O_3 (based on monthly concentration averages) varied $<10\%$. The whole-troposphere $\Delta_{36,Tequil}$ value varied 0.03‰ in $\Delta_{36,Tequil}$ over this range in O_3, with lower O_3 tropopause thresholds yielding lower $\Delta_{36,Tequil}$ values. Resulting variations in steady state $\Delta_{36,trop}$ values were ~0.01‰. The dynamical tropopause definitions yielded nearly identical results to those defined by O_3 concentration at 150 ppb ($V_{trop} = 6.8 \times 10^{18}$ m^3). Our clumped-isotope measurements are consistent with a chemical tropopause of ~150 ppb O_3 with a $\Delta_{36,strat}$ of 2.3‰.

A2. Residence Times in Tropospheric Boxes

The mass- and residence-time weighting for the calculation of E_{trop} and whole-troposphere T_{equil} was used to account for two effects: (i) air mass in each grid box varies with its size and (ii) isotope equilibration toward $\Delta_{36,Tequil}$ in a given grid box depends on the reaction rate and the residence time of air in that grid box. Accounting for (i) is straightforward—weight each box by the mass contained within it—but accounting for (ii) is more difficult. At a dynamic steady state, assuming ergodicity, the exponentially decreasing density profile of air indicates that air spends more time at low altitudes than at high altitudes; it is kept near the surface by the gravitational potential of the Earth. Its residence time in a given grid box, however, depends on time-varying meteorological fields. While a full Lagrangian trajectory study is ideal for tracking an O_2

molecule's transport history, the calculations are too expensive at present for the >3 year long trajectories in a global chemical-transport model required to model $\Delta_{36,T\text{equil}}$ values accurately [*Owen and Honrath*, 2009]. Therefore, we approximate the aggregated Lagrangian residence times in tropospheric grid boxes, relative to each other, using the air density in each box. The air densities reflect the average large-scale behavior at a dynamic steady state, which is appropriate for the multiannual timescales relevant to tropospheric isotope exchange chemistry. Because there is an upper limit for air densities (globally speaking, i.e., surface conditions) and not for residence times, however, our calculated relative residence times at the surface may underestimate the true relative residence times. If so, warm surface temperatures may be underweighted, leading to whole-troposphere $\Delta_{36,T\text{equil}}$ values that are too high.

A3. Oxygen Cycling by the Biosphere

Rates of oxygen production and consumption (3.43×10^{16} mol O_2 yr^{-1} [*Blunier et al.*, 2012]) are 400 times slower than the calculated rate of isotopic equilibration (1.4×10^{19} mol O_2 yr^{-1}). Using the biological end-member of $\Delta_{36}\sim0$ obtained from a earlier closed-system terrarium study and the global box model for Δ_{36} described in *Yeung et al.* [2012], we calculate that biological O_2 cycling affects tropospheric Δ_{36} by approximately −0.01‰ in steady state.

Acknowledgments
We thank A.M. Fiore (Columbia University) for computational resources for simulations, S. Donnelly and R. Hendershot for engineering support, and I. Mellor-Crummey and S. Li for their efforts in construction and testing of the automated O_2 sample preparation system at Rice. We also thank D.R. Blake for providing sample aliquots from the DC3 campaign, M. Bender for providing the sample of 1992 air from Niwot Ridge, CO, and M. Aydin and two anonymous reviewers for comments that improved the manuscript. Finally, we thank the staff of the Cape Grim Baseline Air Pollution Station for their diligence in collecting the air archive samples, and the Australian Bureau of Meteorology for their long-term, and ongoing support of the Cape Grim Air Archive. This work was supported in part by the National Science Foundation (EAR-1049655 and DGE-1144087), the National Aeronautics and Space Administration Upper Atmosphere Research Program (NNX13AH10G) and Cosmochemistry Program, the Deep Carbon Observatory, and Rice University faculty startup funds. The laboratory data reported in this study are freely available as supporting information (Table S1).

References

Anderson, S. M., F. S. Klein, and F. Kaufman (1985), Kinetics of the isotope exchange reaction of ^{18}O with NO and O_2 at 298 K, *J. Chem. Phys.*, *83*(4), 1648–1656.

Appenzeller, C., J. R. Holton, and K. H. Rosenlof (1996), Seasonal variation of mass transport across the tropopause, *J. Geophys. Res.*, *101*(D10), 15,071–15,078, doi:10.1029/96JD00821.

Auvray, M., and I. Bey (2005), Long-range transport to Europe: Seasonal variations and implications for the European ozone budget, *J. Geophys. Res.*, *110*, D11303, doi:10.1029/2004JD005503.

Barth, M. C., et al. (2015), The Deep Convective Clouds and Chemistry (DC3) field campaign, *Bull. Am. Meteorol. Soc.*, *96*, 1281–1309, doi:10.1175/BAMS-D-13-00290.1.

Bender, M., T. Sowers, and L. Labeyrie (1994), The Dole effect and its variations during the last 130,000 years as measured in the Vostok ice core, *Global Biogeochem. Cycles*, *8*(3), 363–376, doi:10.1029/94GB00724.

Bloom, S., et al. (2005), Documentation and Validation of the Goddard Earth Observing System (GEOS) Data Assimilation System—Version 4, in *Technical Report Series on Global Modeling and Data Assimilation*, edited by M. J. Suarez, NASA Goddard Space Flight Center, Greenbelt, Md.

Blunier, T., M. L. Bender, B. Barnett, and J. C. von Fischer (2012), Planetary fertility during the past 400 ka based on the triple isotope composition of O_2 in trapped gases from the Vostok ice core, *Clim. Past*, *8*, 1509–1526, doi:10.5194/cp-8-1509-2012.

Boering, K. A., S. C. Wofsy, B. C. Daube, H. R. Schneider, M. Loewenstein, J. R. Podolske, and T. J. Conway (1996), Stratospheric mean ages and transport rates from observations of carbon dioxide and nitrous oxide, *Science*, *274*(5291), 1340–1343.

Bony, S., et al. (2015), Clouds, circulation and climate sensitivity, *Nat. Geosci.*, *8*(4), 261–268, doi:10.1038/ngeo2398.

Bouwman, A. F., D. S. Lee, D. S. Lee, W. A. H. Asman, F. J. Dentener, K. W. VanderHoek, and J. G. J. Olivier (1997), A global high-resolution emission inventory for ammonia, *Global Biogeochem. Cycles*, *11*(4), 561–587, doi:10.1029/97GB02266.

Brasseur, G., M. H. Hitchman, S. Walters, M. Dymek, E. Falise, and M. Pirre (1990), An interactive chemical dynamic radiative 2-dimensional model of the middle atmosphere, *J. Geophys. Res.*, *95*(D5), 5639–5655, doi:10.1029/JD095iD05p05639.

Butchart, N., et al. (2006), Simulations of anthropogenic change in the strength of the Brewer–Dobson circulation, *Clim. Dyn.*, *27*(7), 727–741, doi:10.1007/s00382-006-0162-4.

Cooper, O. R., et al. (2014), Global distribution and trends of atmospheric ozone: An observation-based review, *Elementa*, *2*, 000029, doi:10.12952/journal.elementa.000029.

Eagle, R. A., C. Risi, J. L. Mitchell, J. M. Eiler, U. Seibt, J. D. Neelin, G. Li, and A. K. Tripati (2013), High regional climate sensitivity over continental China constrained by glacial-recent changes in temperature and the hydrological cycle, *Proc. Natl. Acad. Sci. U.S.A.*, *110*(22), 8813–8818, doi:10.1073/pnas.1213366110.

Eastham, S. D., D. K. Weisenstein, and S. R. H. Barrett (2014), Development and evaluation of the unified tropospheric–stratospheric chemistry extension (UCX) for the global chemistry-transport model GEOS-Chem, *Atmos. Environ.*, *89*, 52–63, doi:10.1016/j.atmosenv.2014.02.001.

Froidevaux, L., et al. (2006), Early validation analyses of atmospheric profiles from EOS MLS on the Aura satellite, *IEEE Trans. Geosci. Remote Sens.*, *44*(5), 1106–1121.

Guenther, A. B., C. L. Heald, L. K. Emmons, and X. Wang (2012), The Model of Emissions of Gases and Aerosols from Nature version 2.1 (MEGAN2.1): An extended and updated framework for modeling biogenic emissions, *Geosci. Model Dev.*, *5*(6), 1471–1492, doi:10.5194/gmd-5-1471-2012.

Haigh, J. D. (1996), The Impact of Solar Variability on Climate, *Science*, *272*(5264), 981–984, doi:10.1126/science.272.5264.981.

Hsu, J., M. J. Prather, and O. Wild (2005), Diagnosing the stratosphere-to-troposphere flux of ozone in a chemistry transport model, *J. Geophys. Res.*, *110*, D19305, doi:10.1029/2005JD006045.

Hudman, R. C., N. E. Moore, A. K. Mebust, R. V. Martin, A. R. Russell, L. C. Valin, and R. C. Cohen (2012), Steps towards a mechanistic model of global soil nitric oxide emissions: Implementation and space based-constraints, *Atmos. Chem. Phys.*, *12*(16), 7779–7795, doi:10.5194/acp-12-7779-2012.

Kuhns, H., E. M. Knipping, and J. M. Vukovich (2005), Development of a United States–Mexico Emissions Inventory for the Big Bend Regional Aerosol and Visibility Observational (BRAVO) Study, *J. Air Waste Manage. Assoc.*, *55*(5), 677–692, doi:10.1080/10473289.2005.10464648.

Langenfelds, R. L., P. J. Fraser, R. J. Francey, L. P. Steele, L. W. Porter, and C. E. Allison (1996), The Cape Grim Air Archive: The first seventeen years, 1978-1995, in *Baseline Atmospheric Program (Australia) 1994-95*, edited by R. J. Francey, A. L. Dick, and N. Derek, pp. 53–70, Bureau of Meteorology, and CSIRO Division of Atmospheric Research, Melbourne, Australia.

Leibensperger, E. M., L. J. Mickley, D. J. Jacob, W. T. Chen, J. H. Seinfeld, A. Nenes, P. J. Adams, D. G. Streets, N. Kumar, and D. Rind (2012), Climatic effects of 1950-2050 changes in US anthropogenic aerosols—Part 1: Aerosol trends and radiative forcing, *Atmos. Chem. Phys.*, *12*(7), 3333–3348, doi:10.5194/acp-12-3333-2012.

Lelli, L., A. A. Kokhanovsky, V. V. Rozanov, M. Vountas, and J. P. Burrows (2014), Linear trends in cloud top height from passive observations in the oxygen A-band, *Atmos. Chem. Phys.*, *14*(11), 5679–5692, doi:10.5194/acp-14-5679-2014.

Liang, M.-C., G. A. Blake, B. R. Lewis, and Y. L. Yung (2007), Oxygen isotopic composition of carbon dioxide in the middle atmosphere, *Proc. Natl. Acad. Sci. U.S.A.*, *104*(1), 21–25.

Liu, G., J. Liu, D. W. Tarasick, V. E. Fioletov, J. J. Jin, O. Moeini, X. Liu, C. E. Sioris, and M. Osman (2013a), A global tropospheric ozone climatology from trajectory-mapped ozone soundings, *Atmos. Chem. Phys.*, *13*(21), 10,659–10,675, doi:10.5194/acp-13-10659-2013.

Liu, J., J. A. Logan, D. B. A. Jones, N. J. Livesey, I. Megretskaia, C. Carouge, and P. Nedelec (2010), Analysis of CO in the tropical troposphere using Aura satellite data and the GEOS-Chem model: Insights into transport characteristics of the GEOS meteorological products, *Atmos. Chem. Phys.*, *10*, 12,207–12,232, doi:10.5194/acp-10-12207-2010.

Liu, J., J. A. Logan, L. T. Murray, H. C. Pumphrey, M. J. Schwartz, and I. A. Megretskaia (2013b), Transport analysis and source attribution of seasonal and interannual variability of CO in the tropical upper troposphere and lower stratosphere, *Atmos. Chem. Phys.*, *13*, 129–146, doi:10.5194/acp-13-129-2013.

Logan, J. A., et al. (2012), Changes in ozone over Europe: Analysis of ozone measurements from sondes, regular aircraft (MOZAIC) and alpine surface sites, *J. Geophys. Res.*, *117*, D09301, doi:10.1029/2011JD016952.

Lueb, R. A., D. H. Ehhalt, and L. E. Heidt (1975), Balloon-borne low temperature air sampler, *Rev. Sci. Instrum.*, *46*(6), 702–705.

Marenco, A., H. Gouget, P. Nédélec, and J.-P. Pagés (1994), Evidences of a long-term increase in tropospheric ozone from Pic du Midi data series: Consequences: Positive radiative forcing, *J. Geophys. Res.*, *99*(D8), 16,617–16,632, doi:10.1029/94JD00021.

MARGO Project Members (2009), Constraints on the magnitude and patterns of ocean cooling at the Last Glacial Maximum, *Nat. Geosci.*, *2*(2), 127–132, doi:10.1038/ngeo411.

Mayewski, P. A., L. D. Meeker, M. S. Twickler, S. Whitlow, Q. Yang, W. B. Lyons, and M. Prentice (1997), Major features and forcing of high-latitude northern hemisphere atmospheric circulation using a 110,000-year-long glaciochemical series, *J. Geophys. Res.*, *102*(C12), 26,345–26,366, doi:10.1029/96JC03365.

Mitovski, T., I. Folkins, R. V. Martin, and M. Cooper (2012), Testing convective transport on short time scales: Comparisons with mass divergence and ozone anomaly patterns about high rain events, *J. Geophys. Res.*, *117*, D02109, doi:10.1029/2011JD016321.

Mote, P. W., K. H. Rosenlof, M. E. McIntyre, E. S. Carr, J. C. Gille, J. R. Holton, J. S. Kinnersley, H. C. Pumphrey, J. M. Russell, and J. W. Waters (1996), An atmospheric tape recorder: The imprint of tropical tropopause temperatures on stratospheric water vapor, *J. Geophys. Res.*, *101*(D2), 3989–4006, doi:10.1029/95JD03422.

Murray, L. T., D. J. Jacob, J. A. Logan, R. C. Hudman, and W. J. Koshak (2012), Optimized regional and interannual variability of lightning in a global chemical transport model constrained by LIS/OTD satellite data, *J. Geophys. Res.*, *117*, D20307, doi:10.1029/2012JD017934.

Murray, L. T., J. A. Logan, and D. J. Jacob (2013), Interannual variability in tropospheric ozone and OH: The role of lightning, *J. Geophys. Res. Atmos.*, *118*, 11,468–11,480, doi:10.1002/jgrd.50857.

Murray, L. T., L. J. Mickley, J. O. Kaplan, E. D. Sofen, M. Pfeiffer, and B. Alexander (2014), Factors controlling variability in the oxidative capacity of the troposphere since the Last Glacial Maximum, *Atmos. Chem. Phys.*, *14*, 3589–3622.

Neu, J. L., T. Flury, G. L. Manney, M. L. Santee, N. J. Livesey, and J. Worden (2014), Tropospheric ozone variations governed by changes in stratospheric circulation, *Nat. Geosci.*, *7*, 340–344, doi:10.1038/ngeo2138.

Newman, P. A., et al. (2002), An overview of the SOLVE/THESEO 2000 campaign, *J. Geophys. Res.*, *107*(D20), 8259, doi:10.1029/2001JD001303.

Oberländer-Hayn, S., et al. (2016), Is the Brewer-Dobson circulation increasing or moving upward? *Geophys. Res. Lett.*, *43*, 1772–1779, doi:10.1002/2015GL067545.

Olivier, J. G. J., J. A. van Aardenne, F. J. Dentener, V. Pagliari, L. N. Ganzeveld, and J. A. H. W. Peters (2005), Recent trends in global greenhouse gas emissions: Regional trends 1970–2000 and spatial distribution of key sources in 2000, *Environ. Sci.*, *2*(2–3), 81–99, doi:10.1080/15693430500400345.

Orbe, C., M. Holzer, L. M. Polvani, D. W. Waugh, F. Li, L. D. Oman, and P. A. Newman (2014), Seasonal ventilation of the stratosphere: Robust diagnostics from one-way flux distributions, *J. Geophys. Res. Atmos.*, *119*, 293–306, doi:10.1002/2013JD020213.

Oster, J. L., D. E. Ibarra, M. J. Winnick, and K. Maher (2015), Steering of westerly storms over western North America at the Last Glacial Maximum, *Nat. Geosci.*, *8*(3), 201–205, doi:10.1038/ngeo2365.

Owen, R. C., and R. E. Honrath (2009), Technical note: A new method for the Lagrangian tracking of pollution plumes from source to receptor using gridded model output, *Atmos. Chem. Phys.*, *9*(7), 2577–2595, doi:10.5194/acp-9-2577-2009.

Pan, L. L., W. J. Randel, B. L. Gary, M. J. Mahoney, and E. J. Hintsa (2004), Definitions and sharpness of the extratropical tropopause: A trace gas perspective, *J. Geophys. Res.*, *109*, D23103, doi:10.1029/2004JD004982.

Pan, L. L., et al. (2014), Thunderstorms enhance tropospheric ozone by wrapping and shedding stratospheric air, *Geophys. Res. Lett.*, *41*, 7785–7790, doi:10.1002/2014GL061921.

Park, S., et al. (2007), The CO_2 tracer clock for the Tropical Tropopause Layer, *Atmos. Chem. Phys.*, *7*, 3989–4000.

Partin, J. W., K. M. Cobb, J. F. Adkins, B. Clark, and D. P. Fernandez (2007), Millennial-scale trends in west Pacific warm pool hydrology since the Last Glacial Maximum, *Nature*, *449*(7161), 452–455, doi:10.1038/nature06164.

Plumb, R. A. (2007), Tracer interrelationships in the stratosphere, *Rev. Geophys.*, *45*, RG4005, doi:10.1029/2005RG000179.

Plumb, R. A., and M. K. W. Ko (1992), Interrelationships between mixing ratios of long-lived stratospheric constituents, *J. Geophys. Res.*, *97*(D9), 10,145–10,156, doi:10.1029/92JD00450.

Rienecker, M. M., et al. (2011), MERRA: NASA's Modern-Era Retrospective Analysis for Research and Applications, *J. Clim.*, *24*(14), 3624–3648, doi:10.1175/jcli-d-11-00015.1.

Risi, C., S. Bony, F. Vimeux, and J. Jouzel (2010), Water-stable isotopes in the LMDZ4 general circulation model: Model evaluation for present-day and past climates and applications to climatic interpretations of tropical isotopic records, *J. Geophys. Res.*, *115*, D12118, doi:10.1029/2009JD013255.

Santer, B. D., et al. (2003), Contributions of anthropogenic and natural forcing to recent tropopause height changes, *Science*, *301*, 479–483.

Santer, B. D., et al. (2013), Human and natural influences on the changing thermal structure of the atmosphere, *Proc. Natl. Acad. Sci. U.S.A.*, *110*(43), 17,235–17,240.

Schneider, T., P. A. O'Gorman, and X. J. Levine (2010), Water vapor and the dynamics of climate changes, *Rev. Geophys.*, *48*, RG3001, doi:10.1029/2009RG000302.

Schoeberl, M. R. (2004), Extratropical stratosphere-troposphere mass exchange, *J. Geophys. Res.*, *109*, D13303, doi:10.1029/2004JD004525.

Schoeberl, M. R., B. N. Duncan, A. R. Douglass, J. Waters, N. Livesey, W. Read, and M. Filipiak (2006), The carbon monoxide tape recorder, *Geophys. Res. Lett.*, *33*, L12811, doi:10.1029/2006GL026178.
Schroeder, J. R., L. L. Pan, T. Ryerson, G. Diskin, J. Hair, S. Meinardi, I. Simpson, B. Barletta, N. Blake, and D. R. Blake (2014), Evidence of mixing between polluted convective outflow and stratospheric air in the upper troposphere during DC3, *J. Geophys. Res. Atmos.*, *119*, 11,477–11,491, doi:10.1002/2014JD022109.
Schultz, M. G., et al. (2007), REanalysis of the TROpospheric chemical composition over the past 40 years (RETRO) — A long-term global modeling study of tropospheric chemistry Rep., Max Planck Institute for Meteorology, Jülich/Hamburg, Germany.
Seidel, D. J., R. J. Ross, J. K. Angell, and G. C. Reid (2001), Climatological characteristics of the tropical tropopause as revealed by radiosondes, *J. Geophys. Res.*, *106*(D8), 7857–7878, doi:10.1029/2000JD900837.
Severinghaus, J. P., R. Beaudette, M. A. Headly, K. Taylor, and E. J. Brook (2009), Oxygen-18 of O_2 Records the Impact of Abrupt Climate Change on the Terrestrial Biosphere, *Science*, *324*(5933), 1431–1434.
Shepherd, T. G. (2014), Atmospheric circulation as a source of uncertainty in climate change projections, *Nat. Geosci.*, *7*(10), 703–708, doi:10.1038/ngeo2253.
Sherwood, S. C., S. Bony, and J.-L. Dufresne (2014), Spread in model climate sensitivity traced to atmospheric convective mixing, *Nature*, *505*(7481), 37–42, doi:10.1038/nature12829.
Shindell, D. T., G. A. Schmidt, M. E. Mann, D. Rind, and A. Waple (2001), Solar Forcing of Regional Climate Change During the Maunder Minimum, *Science*, *294*(5549), 2149–2152, doi:10.1126/science.1064363.
Škerlak, B., M. Sprenger, and H. Wernli (2014), A global climatology of stratosphere-troposphere exchange using the ERA-Interim data set from 1979–2011, *Atmos. Chem. Phys.*, *14*, 913–937, doi:10.5194/acp-14-913-2014.
Stansell, N. D., P. J. Polissar, and M. B. Abbott (2007), Last glacial maximum equilibrium-line altitude and paleo-temperature reconstructions for the Cordillera de Mérida, Venezuelan Andes, *Quat. Res.*, *67*, 115–127.
Stettler, M. E. J., S. D. Eastham, and S. R. H. Barrett (2011), Air quality and public health impacts of UK airports. Part I: Emissions, *Atmos. Environ.*, *45*(31), 5415–5424, doi:10.1016/j.atmosenv.2011.07.012.
Stevenson, D. S., et al. (2013), Tropospheric ozone changes, radiative forcing and attribution to emissions in the Atmospheric Chemistry and Climate Model Intercomparison Project (ACCMIP), *Atmos. Chem. Phys.*, *13*, 3063–3085, doi:10.5194/acp-13-3063-2013.
Stohl, A., H. Wernli, P. James, M. Bourqui, C. Forster, M. A. Liniger, P. Seibert, and M. Sprenger (2003), A new perspective of stratosphere-troposphere exchange, *Bull. Am. Meteorol. Soc.*, *84*, 1565–1573, doi:10.1175/BAMS-84-11-1565.
Streets, D. G., Q. Zhang, L. Wang, K. He, J. Hao, Y. Wu, Y. Tang, and G. R. Carmichael (2006), Revisiting China's CO emissions after the Transport and Chemical Evolution over the Pacific (TRACE-P) mission: Synthesis of inventories, atmospheric modeling, and observations, *J. Geophys. Res.*, *111*, D14306, doi:10.1029/2006JD007118.
Sudo, K., and M. Takahashi (2001), Simulation of tropospheric ozone changes during 1997–1998 El Niño: Meteorological impact on tropospheric photochemistry, *Geophys. Res. Lett.*, *28*(21), 4091–4094, doi:10.1029/2001GL013335.
Sullivan, J. T., T. J. McGee, A. M. Thompson, R. B. Pierce, G. K. Sumnicht, L. W. Twigg, E. Eloranta, and R. M. Hoff (2015), Characterizing the lifetime and occurrence of stratospheric-tropospheric exchange events in the rocky mountain region using high-resolution ozone measurements, *J. Geophys. Res. Atmos.*, *120*, 12,410–12,424, doi:10.1002/2015JD023877.
Sun, W., P. Hess, and B. Tian (2014), The response of the equatorial tropospheric ozone to the Madden–Julian Oscillation in TES satellite observations and CAM-chem model simulation, *Atmos. Chem. Phys.*, *14*(21), 11,775–11,790, doi:10.5194/acp-14-11775-2014.
Thiemens, M. H., T. Jackson, E. C. Zipf, P. W. Erdman, and C. van Egmond (1995), Carbon Dioxide and Oxygen Isotope Anomalies in the Mesosphere and Stratosphere, *Science*, *270*(5238), 969–972.
Thompson, L. G., E. Mosley-Thompson, M. E. Davis, P.-N. Lin, K. A. Henderson, J. Cole-Dai, J. F. Bolzan, and K.-b. Liu (1995), Late glacial stage and Holocene tropical ice core records from Huarascarán, Peru, *Science*, *269*, 46–50.
Tian, B., Y. L. Yung, D. E. Waliser, T. Tyranowski, L. Kuai, E. J. Fetzer, and F. W. Irion (2007), Intraseasonal variations of the tropical total ozone and their connection to the Madden-Julian Oscillation, *Geophys. Res. Lett.*, *34*, L08704, doi:10.1029/2007GL029451.
Tripati, A. K., S. Sahany, D. Pittman, R. A. Eagle, J. D. Neelin, J. L. Mitchell, and L. Beaufort (2014), Modern and glacial tropical snowlines controlled by sea surface temperature and atmospheric mixing, *Nat. Geosci.*, *7*, 205–209.
van der Werf, G. R., J. T. Randerson, L. Giglio, G. J. Collatz, M. Mu, P. S. Kasibhatla, D. C. Morton, R. S. DeFries, Y. Jin, and T. T. van Leeuwen (2010), Global fire emissions and the contribution of deforestation, savanna, forest, agricultural, and peat fires (1997–2009), *Atmos. Chem. Phys.*, *10*(23), 11,707–11,735, doi:10.5194/acp-10-11707-2010.
van Donkelaar, A., et al. (2008), Analysis of aircraft and satellite measurements from the Intercontinental Chemical Transport Experiment (INTEX-B) to quantify long-range transport of East Asian sulfur to Canada, *Atmos. Chem. Phys.*, *8*(11), 2999–3014, doi:10.5194/acp-8-2999-2008.
Vecchi, G. A., B. J. Soden, A. T. Wittenberg, I. M. Held, A. Leetmaa, and M. J. Harrison (2006), Weakening of tropical Pacific atmospheric circulation due to anthropogenic forcing, *Nature*, *441*(7089), 73–76, doi:10.1038/nature04744.
Vinken, G. C. M., K. F. Boersma, D. J. Jacob, and E. W. Meijer (2011), Accounting for non-linear chemistry of ship plumes in the GEOS-Chem global chemistry transport model, *Atmos. Chem. Phys.*, *11*(22), 11,707–11,722, doi:10.5194/acp-11-11707-2011.
Virts, K. S., and J. M. Wallace (2014), Observations of Temperature, Wind, Cirrus, and Trace Gases in the Tropical Tropopause Transition Layer during the MJO, *J. Atmos. Sci.*, *71*(3), 1143–1157, doi:10.1175/JAS-D-13-0178.1.
Volz, A., and D. Kley (1988), Evaluation of the Montsouris series of ozone measurements made in the nineteenth century, *Nature*, *332*, 240–242.
Wang, Y. H., and D. J. Jacob (1998), Anthropogenic forcing on tropospheric ozone and OH since preindustrial times, *J. Geophys. Res.*, *103*(D23), 31,123–31,135, doi:10.1029/1998JD100004.
Wang, Y. J., H. Cheng, R. L. Edwards, X. G. Kong, X. H. Shao, S. T. Chen, J. Y. Wu, X. Y. Jiang, X. F. Wang, and Z. S. An (2008), Millennial- and orbital-scale changes in the East Asian monsoon over the past 224,000 years, *Nature*, *451*(7182), 1090–1093, doi:10.1038/nature06692.
Wang, Z., E. A. Schauble, and J. M. Eiler (2004), Equilibrium thermodynamics of multiply substituted isotopologues of molecular gases, *Geochim. Cosmochim. Acta*, *68*(23), 4779–4797.
Waugh, D. W., and L. M. Polvani (2000), Climatology of intrusions into the tropical upper troposphere, *Geophys. Res. Lett.*, *27*(23), 3857–3860, doi:10.1029/2000GL012250.
Waugh, D. W., et al. (2013), Tropospheric SF_6: Age of air from the Northern Hemisphere midlatitude surface, *J. Geophys. Res. Atmos.*, *118*, 11,429–11,441, doi:10.1002/jgrd.50848.
Wiegel, A. A., A. S. Cole, K. J. Hoag, E. L. Atlas, S. M. Schauffler, and K. A. Boering (2013), Unexpected variations in the triple oxygen isotope composition of stratospheric carbon dioxide, *Proc. Natl. Acad. Sci. U.S.A.*, *110*(44), 17,680–17,685.
Wiegell, M. R., N. W. Larsen, T. Pedersen, and H. Egsdard (1997), The temperature dependence of the exchange reaction between oxygen atoms and dioxygen molecules studied by means of isotopes and spectroscopy, *Int. J. Chem. Kinet.*, *29*(10), 745–753.

Wofsy, S. C. (2011), HIAPER Pole-to-Pole Observations (HIPPO): Fine-grained, global-scale measurements of climatically important atmospheric gases and aerosols, *Philos. Trans. R. Soc. A*, *369*, 2073–2086, doi:10.1098/rsta.2010.0313.

Wu, S., L. J. Mickley, D. J. Jacob, J. A. Logan, R. M. Yantosca, and D. Rind (2007), Why are there large differences between models in global budgets of tropospheric ozone? *J. Geophys. Res.*, *112*, D05302, doi:10.1029/2006JD007801.

Xiao, Y., J. A. Logan, D. J. Jacob, R. C. Hudman, R. M. Yantosca, and D. R. Blake (2008), Global budget of ethane and regional constraints on US sources, *J. Geophys. Res.*, *113*, D21306, doi:10.1029/2007JD009415.

Yeung, L. Y., H. P. Affek, K. J. Hoag, W. Guo, A. A. Wiegel, E. L. Atlas, S. M. Schauffler, M. Okumura, K. A. Boering, and J. M. Eiler (2009), Large and unexpected enrichment in stratospheric $^{16}O^{13}C^{18}O$ and its meridional variation, *Proc. Natl. Acad. Sci. U.S.A.*, *106*(28), 11,496–11,501.

Yeung, L. Y., E. D. Young, and E. A. Schauble (2012), Measurements of $^{18}O^{18}O$ and $^{17}O^{18}O$ in the atmosphere and the influence of isotope-exchange reactions, *J. Geophys. Res.*, *117*, D18306, doi:10.1029/2012JD017992.

Yeung, L. Y., J. L. Ash, and E. D. Young (2014), Rapid photochemical equilibration of isotope bond ordering in O_2, *J. Geophys. Res. Atmos.*, *119*, 10,552–10,566, doi:10.1002/2014JD021909.

Yeung, L. Y., J. L. Ash, and E. D. Young (2015), Biological signatures in clumped isotopes of O_2, *Science*, *348*(6233), 431–434, doi:10.1126/science.aaa6284.

Yoshimura, K., M. Kanamitsu, D. Noone, and T. Oki (2008), Historical isotope simulation using Reanalysis atmospheric data, *J. Geophys. Res.*, *113*, D19108, doi:10.1029/2008JD010074.

Young, P. J., et al. (2013), Pre-industrial to end 21st century projections of tropospheric ozone from the Atmospheric Chemistry and Climate Model Intercomparison Project (ACCMIP), *Atmos. Chem. Phys.*, *13*, 2063–2090.

Ziemke, J. R., and S. Chandra (2003a), La Nina and El Nino—induced variabilities of ozone in the tropical lower atmosphere during 1970–2001, *Geophys. Res. Lett.*, *30*(3), 1142, doi:10.1029/2002GL016387.

Ziemke, J. R., and S. Chandra (2003b), A Madden-Julian Oscillation in tropospheric ozone, *Geophys. Res. Lett.*, *30*(23), 2182, doi:10.1029/2003GL018523.

Ziemke, J. R., A. R. Douglass, L. D. Oman, S. E. Strahan, and B. N. Duncan (2015), Tropospheric ozone variability in the tropics from ENSO to MJO and shorter timescales, *Atmos. Chem. Phys.*, *15*(14), 8037–8049, doi:10.5194/acp-15-8037-2015.